Experimental Gerontology 181 (2023) 112269

Contents lists available at ScienceDirect

Experimental Gerontology

journal homepage: www.elsevier.com/locate/expgero

Vutiglabridin exerts anti-ageing effects in aged mice through alleviating age-related metabolic dysfunctions

Jooseung Hyeon [a,1], Jihan Lee [a,1], Eunju Kim [b,c], Hyeong Min Lee [b,c,d], Kwang Pyo Kim [b,c], Jaejin Shin [d], Hyung Soon Park [d], Yun-Il Lee [e], Chang-Hoon Nam [a,*]

[a] Aging and Immunity Laboratory, Department of New Biology, Daegu Gyeongbuk Institute of Science and Technology, Daegu 42988, Republic of Korea
[b] Department of Applied Chemistry, Institute of Natural Science, Global Center for Pharmaceutical Ingredient Materials, Kyung Hee University, Yongin, Republic of Korea
[c] Department of Biomedical Science and Technology, Kyung Hee Medical Science Research Institute, Kyung Hee University, Seoul, Republic of Korea
[d] Glaceum Incorporation, Research Department, Suwon, Republic of Korea
[e] Well Aging Research Center, Division of Biotechnology, Department of Interdisciplinary Studies, Daegu Gyeongbuk Institute of Science and Technology, Daegu, Republic of Korea

ARTICLE INFO

Section Editor: Cheryl Conover

Keywords:
Ageing
Metabolism
Mitochondrial homeostasis
Inflammageing

ABSTRACT

Background: Ageing alters the ECM, leading to mitochondrial dysfunction and oxidative stress, which triggers an inflammatory response that exacerbates with age. Age-related changes impact satellite cells, affecting muscle regeneration, and the balance of proteins. Furthermore, ageing causes a decline in NAD^+ levels, and alterations in fat metabolism that impact our health. These various metabolic issues become intricately intertwined with ageing, leading to a variety of individual-level diseases and profoundly affecting individuals' healthspan. Therefore, we hypothesize that vutiglabridin capable of alleviating these metabolic abnormalities will be able to ameliorate many of the problems associated with ageing.

Method: The efficacy of vutiglabridin, which alleviates metabolic issues by enhancing mitochondrial function, was assessed in aged mice treated with vutiglabridin and compared to untreated elderly mice. On young mice, vutiglabridin-treated aged mice, and non-treated aged mice, the Senescence-associated beta-galactosidase staining and q-PCR for ageing marker genes were carried out. Bulk RNA-seq was carried out on GA muscle, eWAT, and liver from each group of mice to compare differences in gene expression in various gene pathways. Blood from each group of mice was used to compare and analyze the ageing lipid profile.

Results: SA-β-gal staining of eWAT, liver, kidney, and spleen of ageing mice showed that vutiglabridin had anti-ageing effects compared to the control group, and q-PCR of ageing marker genes including *Cdkn1a* and *Cdkn2a* in each tissue showed that vutiglabridin reduced the ageing process. In aged mice treated with vutiglabridin, GA muscle showed improved homeostasis compared to controls, eWAT showed restored insulin sensitivity and prevented FALC-induced inflammation, and liver showed reduced inflammation levels due to prevented TLO formation, improved mitochondrial complex I assembly, resulting in reduced ROS formation. Furthermore, blood lipid analysis revealed that ageing-related lipid profile was relieved in ageing mice treated with vutiglabridin versus the control group.

Conclusion: Vutiglabridin slows metabolic ageing mechanisms such as decreased insulin sensitivity, increased inflammation, and altered NAD^+ metabolism in adipose tissue in mice experiments, while also retaining muscle homeostasis, which is deteriorated with age. It also improves the lipid profile in the blood and restores mitochondrial function in the liver to reduce ROS generation.

Abbreviations: ECM, extracellular matrix; eWAT, epididymal white adipose tissue; SA-β-gal, Senescence-associated beta-galactosidase; FALCs, fat-associated lymphoid clusters; TLOs, Tertiary lymphoid organs; ROS, reactive oxygen species; OXPHOS, oxidative phosphorylation; VAT, visceral adipose tissue; ATMs, adipose tissue macrophages; HDF, human dermal fibroblast; TMSD, Trimethylsilyldiazomethane; DEGs, differentially expressed genes; GO, gene ontology; UPR, unfolded protein response; DAMPs, damage-associated molecular patterns; PRRs, pattern recognition receptors; TLRs, Toll-like receptors; ETC, electron transport chain.

* Corresponding author.
E-mail address: chang@dgist.ac.kr (C.-H. Nam).

[1] These two authors have contributed equally and share the first authorship.

https://doi.org/10.1016/j.exger.2023.112269
Received 31 March 2023; Received in revised form 7 August 2023; Accepted 8 August 2023
Available online 1 September 2023

1. Introduction

Ageing is an unavoidable process marked by the accumulation of molecular and cellular damage, which leads to increased prevalence and mortality (Aunan et al., 2016; Melzer et al., 2020). Longevity has increased as civilization has progressed, but healthspan has not improved as much as lifespan (Crimmins, 2015), which poses a significant challenge to public health and research (Lutz et al., 2008). Furthermore, as life expectancy rises, ageing becomes the leading risk factor for morbidities (Franceschi et al., 2018; Partridge et al., 2018), which can be caused by the gradual decline in metabolism throughout life (Pontzer et al., 2021).

One of the factors that contribute to changes in metabolism during ageing is the alteration of the extracellular matrix (ECM), which is a complex environment that has three layers within skeletal muscle (Csapo et al., 2020; Gattazzo et al., 2014) and accumulates over time due to its long half-life (Moon et al., 2004). This accumulation causes oxidative stress, such as reactive oxygen species (ROS) (Martins et al., 2021; López-Otín et al., 2013), and changes in mitochondrial shape (Kang et al., 2021). The increase in ROS and mitochondrial dysfunction triggers an inflammatory response, which exacerbates with age (López-Armada et al., 2013). The impact of the altered ECM on metabolism has also been linked to mitochondrial dysfunction and oxidative stress (Ge et al., 2021; Bhatti et al., 2017).

Ageing affects our body's metabolism, including the functioning of satellite cells in skeletal muscle regeneration, and the balance of proteins. Research has shown that ageing-related changes in the ECM and impaired mitochondrial function impact satellite cells, which play a crucial role in muscle regeneration (Melouane et al., 2020; Yamakawa et al., 2020). As we age, our bodies become less effective at maintaining the balance of proteins through the chaperones and two protein-degrading systems: the ubiquitin-proteasome and the lysosome-autophagy systems (López-Otín et al., 2013; Tyedmers et al., 2010; Rubinsztein et al., 2011). However, these systems are positively associated with healthy ageing and longevity (Pérez et al., 2009). The accumulation of unfolded proteins and endoplasmic reticulum stress, a common feature of ageing (Kaushik and Cuervo, 2015), can activate signalling pathways like JNK and NF-κB, leading to insulin resistance (Amen et al., 2019).

Ageing also causes a decline in NAD^+ levels, a coenzyme required for energy metabolism (Covarrubias et al., 2021). This decrease is associated with changes in NAD^+ biosynthesis and degradation enzymes (Liu et al., 2018), which promote the onset of age-related diseases, particularly metabolic dysfunction (Covarrubias et al., 2021). And the high glycolytic flux is to meet the NAD^+ requirement under the reduced oxidative phosphorylation (OXPHOS) system. (Feng et al., 2016; Gomes et al., 2013). Further evidence suggests that ageing is associated with lower levels of mitochondrial enzymes (complex I) in hepatocytes, which exacerbates metabolic dysfunction (Navarro and Boveris, 2004).

Alterations in fat metabolism as we age can also have a significant impact on our health. One key factor is the formation of fat-associated lymphoid clusters (FALCs) in visceral adipose tissue (VAT) (Camell et al., 2019), which are facilitated by adipose tissue macrophages (ATMs) (Bénézech et al., 2015; Camell et al., 2017). This process is driven by the activation of the NOD-, LRR- and pyrin domain-containing protein 3 (NLRP3) inflammasome (Martinon et al., 2009; Place and Kanneganti, 2018; Strowig et al., 2012), which is also associated with insulin resistance (He et al., 2020; McNelis and Olefsky, 2014). Specifically, free saturated fatty acids activate Toll-like receptors (TLR2 and TLR4) in ATMs, leading to the production of pro-inflammatory cytokines that attract lymphocytes (Chawla et al., 2011; Kalathookunnel Antony et al., 2018). Additionally, pro-inflammatory macrophages expressing CD38 contribute to age-related metabolic dysfunctions by decreasing tissue NAD levels (Covarrubias et al., 2020; Chini et al., 2020). Lipid species also change with ageing (Montoliu et al., 2014), and they play a significant role in regulating healthspan (Mutlu et al., 2021). Recent research suggests that age-associated lipid species changes are linked to age-related disease (Johnson and Stolzing, 2019).

These age-related changes can impact the prevalence and mortality rates, leading to the development of drugs like metformin and rapamycin to extend life expectancy and improve these metabolic dysfunctions (Podhorecka et al., 2017; Zhang et al., 2021; Amorim et al., 2022). However, since ageing is a multifaceted process caused by a variety of factors in each organ and individual (Benayoun et al., 2019; Stegeman and Weake, 2017; Zhou et al., 2020; Ori et al., 2015), a variety of anti-ageing drugs will have to be developed.

Vutiglabridin is a clinical phase II drug (NCT05197556) that facilitates metabolism by improving mitochondrial function. Vutiglabridin improved mitochondrial function and energy expenditure in mice subjected to excess lipid stress (Choi et al., 2021) and reduced hepatic steatosis and inflammation through antioxidant and autophagy mechanism in non-alcoholic steatosis hepatitis (NASH) mouse model (Shin et al., 2021). Recently, we found that vutiglabridin alleviates the ageing phenotype associated with cellular replication and metabolism in senescent human dermal fibroblast (HDF) (Heo et al., 2023). Based on these findings, we hypothesised that vutiglabridin would alleviate metabolic dysfunctions that occur during the ageing process in mice. To test this hypothesis, we administered vutiglabridin to aged mice and then analyzed various tissues separately to investigate how vutiglabridin affected each tissue and whether it had anti-ageing effects. And we found that vutiglabridin exerts anti-ageing phenotype on tissue-specific effects in aged mice.

2. Materials and methods

2.1. Animal procedures

C57BL/6J wild-type male mice were obtained from the Laboratory Animal Resource Center of the Korea Research Institute of Bioscience and Biotechnology (KRIBB). 20-month-old male mice were fed either 50 mg/kg (mpk) of the vutiglabridin mixed with the diet for 3 months or a normal diet. 2-month-old mice were used as a young control. Weight change was checked once a week. All mice were housed in ventilated cages with constant temperature (20–26 °C) and humidity (40–60 %) under specific pathogen-free (SPF) conditions in a 12:12 h dark/light cycle. All mice also were access to water and food with ad libitum. Each tissue was sampled for analysis after anesthesia with avertin (240 mg/kg). The study was approved by the Ethical Committee of Animal Research of Daegu Gyeongbuk Institute of Science and Technology, Daegu, South Korea (DGIST-IACUC-21070701-00).

2.2. Senescence-associated beta-galactosidase (SA-β-gal) staining

For the SA-β-gal staining, spleen, kidney, liver, and epididymal white adipose tissue (eWAT) were gently washed in PBS to remove excess residual blood and fixed using 4 % paraformaldehyde (PFA) (Biosesang, cat# PC2031-100-00) in 4 °C. Fixed tissues were embedded with OCT compound (Lecia, cat# 3801480) on the mold (Daihan Scientific Group, cat# SP.M475.2) in liquid nitrogen containing isopentane and stored at −80 °C until analysis. The frozen spleen, kidney, and liver were sectioned into 14 μm, maintaining −20 °C by a microtome (Thermo Scientific, cat# CryoStar NX50). The sectioned tissue was sampled in a slide. Put 1 ml of PBS on the slide and wash twice for 5 min to remove OCT. The spleen, kidney, and liver section from which OCT has been removed is stained with 1 ml of SA-β-gal staining solution (40 mM citric acid monohydrate/sodium dihydrogen phosphate monohydrate (Merck, cat# 5949-29-1 and 10049-21-5, respectively) buffer at pH 5.8, 5 mM potassium hexacyanoferrate (II) trihydrate (Merck, cat# 14459-95-1), 5 mM potassium hexacyanoferrate (III) (Merck, cat# 13746-66-2), 150mM sodium chloride (Merck, cat# 7647-14-5), 2 mM magnesium chloride hexahydrate (Merck, cat# 7791-18-6), and 1 mg/ml 5-bromo-4-chloro-3-indolyl-β-D-galactopyranoside (X-gal) (Merck, cat# 7240-90-

6) in distilled water) in a non-CO2 incubator at 37 °C for 5–9.5 h (Jannone et al., 2020). Areas of SA-β-gal staining were randomly captured at least 4 points per subject using a microscope camera and were analyzed by Fiji software using a threshold tool and wound healing tool. 30 mg of eWAT was incubated for 10 h in a 1.5 ml tube containing 1 ml of staining solution at pH 6. Whole eWAT and tissue compressed with two slides were observed to analyze the relative staining activation.

2.3. RNA extraction and real-time PCR

To assess mRNA levels, GA muscle, eWAT, liver, kidney, and spleen were gently washed in PBS to remove excess residual blood, incubated for 1 h at 4 °C in a 1.5 ml tube containing 700ul of RNAlater (ThermoFisher, cat# AM7020), and stored in −80 °C until analysis. After thawing, GA muscle, liver, kidney, and spleen were homogenized with 700 μl of RLT buffer containing β-mercaptoethanol (Merck, cat# 60-24-2) and a zirconium bead 1.5 mm (spleen, kidney, and liver) (Merck, cat# Z763799) or 3.0 mm (GA muscle) (Merck, cat# Z763802) using a bead bug (Merck, cat# Z763705) under 30 s and 4000r.p.m. Tissue homogenate passed through QIAshredder (QIAGEN, cat# 79656) once to remove insoluble debris. The collected solution was purified by RNA using the RNeasy Mini Kit (QIAGEN, cat# 74004) and retrotranscribed to cDNA using TOPscript™ cDNA Synthesis kit (Enzynomics, cat# EZ005S). Real-Time PCR (qPCR) reactions were performed with TOPreal™ qPCR 2× PreMIX (SYBR Green with low ROX) (Enzynomics, cat# RT500M) in a real-time PCR detection system (Bio-Rad, cat# CFX96). *Gapdh* normalized the relative mRNA levels in the eWAT, liver, kidney, and spleen. *Actb* normalized the relative mRNA levels in the GA muscle. Relative expression was calculated as $RQ = 2^{-\Delta\Delta Ct}$. The specific primer sequences are the following:

Gene	Forward primer	Reverse primer
Cdkn1a	5′-GCAGATCCACAGCGATATCCA-3′	5′-AACAGGTCGGACATCACCAG-3′
Cdkn2a	5′-CCCAACGCCCCGAACT-3′	5′-GCAGAAGAGCTGCTACGTGAA-3′
Il6	5′-TGAACAACGATGATGCACTTG-3′	5′-CTGAAGGACTCTGGCTTTGTC-3′
Cxcl2	5′-GAAGTCATAGCCACTCTCAAGG-3′	5′-CCTCCTTTCCAGGTCAGTTAGC-3′
Actb	5’-GTCCACACCCGCCACC-3’	5′-ACCCATTCCCACCATCACAC-3′
Gapdh	5’-CCCTTAAGAGGGATGCTGCC-3’	5′-TACGGCCAAATCCGTTCACA-3′
Klotho	5′-CCTCCTTTACCTGAAAACCAGCC-3′	5′-CCACAGATAGACATTCGGGTCAG-3′
Ppar-γ	5′-GTACTGTCGGTTTCAGAAGTGCC-3′	5′-ATCTCCGCCAACAGCTTCTCCT-3′
J-chain	5′-GGAGAATATCTCTGATCCCACCT-3′	5′-TGTTGCTCTGGGTGGCAGTAAC-3′
Sparc	5′-CACCTGGACTACATCGGACCAT-3′	5′-CTGCTTCTCAGTGAGGAGGTTG-3′

2.4. ELISA

After intracardiac bleeding, blood was collected into the 1.5 ml tube and incubated at room temperature for 30 to 40 min to coagulate. The coagulated blood was centrifuged at 4 °C under 2000 r.p.m. for 15 min to separate serum. Serum IL-6 levels were detected using a mouse interleukin 6 ELISA kit (Cusabio, cat# CSB-E04639m). The one-fifth dilution using the sample diluent was measured at 450 nm wavelength with a microplate reader.

2.5. Glutathione assay

For the glutathione assay, the liver was gently washed in PBS for glutathione assay to remove excess residual blood and immediately stored at −80 °C. After thawing the frozen tissue on ice, 40 mg of the liver was placed in the tube that containing both 1.5 mm beads (Merck, cat# Z763799) and 400 ml of cold buffer (50 mM MES) and then homogenized at 4000 r.p.m. for 30 s using a homogenizer (Merck, cat# Z763705). To remove debris, the homogenated solution was centrifuged at 10,000*g* for 15 min at 4 °C. The supernatant was analyzed for GSH and GSSG using a Glutathione assay kit (Cayman chemical, cat# 703002).

2.6. RNA-sequencing

2.6.1. RNA extraction

Samples were thawed at room temperature and total RNA was extracted using chloroform and Trizol method followed by purification with the GeneAll Hybrid-R™ kit according to the manufacturer's instructions. DNA was inactivated using GeneAll Ribospin™II kit.

2.6.2. Library preparation

Ten nanogram of total RNA was reverse transcribed into cDNA using NGS Reverse Transcription Kit from Thermo Fisher (Cat# A45003). The thermocycling conditions for the reverse transcription were: 10 min at 25 °C, 10 min at 50 °C, and finally 5 min at 85 °C, then a holding temperature of 4 °C.

The barcoded libraries pool was then amplified by using Ion AmpliSeq™ Transcriptome Mouse Gene Expression Chef-Ready Kit (Cat. No. A36412), which allows simultaneous gene expression measurement of over 20,000 mouse Refseq genes. The barcoded libraries were prepared on the Ion Chef ™ system (TermoFisher Scientifc). Library pool concentration was evaluated with a Bio-rad CFX96 using Ion Library TaqMan™ Quantitation Kit. Each barcoded library pool was diluted into 70 pM for template preparation and sequenced on an Ion 540™ chip (Cat# A27766) on the Ion S5 System, according to the manufacturer's protocol.

2.6.3. Data analysis

Torrent suite (TM) software aligns reads to the mouse reference using the Ion Torrent Mapping Alignment Program. The ampliSeqRNA plugin generates an initial summary report on the number of mapped reads.

Raw read count and normalized reads count (RPM, reads per million) were downloaded for the following analysis.

In the next step, statistical analysis was performed in R (ver 4.1.1) using packages available through CRAN (http://cran.r-project.org/) and Bioconductor (http://www.bioconductor.org/). Differentially expressed genes (DEGs) were identified by DESeq2 (ver. 1.34.0) using the DESeq2 function. According to the guide of DESeq2, un-normalized read counts were prepared for the RNA-seq analysis (Love et al., 2014). The scatter plot, volcano plot and heatmap were created using ggplot2 (ver. 3.3.6), limma (ver. 3.50.1) and pheatmap (ver. 1.0.12). Finally, clusterProfiler (ver. 4.0.5) and enrichplot (ver. 1.12.3) were used to perform the Gene Set Enrichment Analysis (GSEA) of Gene Ontology from the L2FCs (Log2 Fold Change) and *p*-values.

2.7. Lipidomics

The serum was sampled by the method mentioned in ELISA. The serum lipid profile was analyzed using LC-MS by professor Kwang-Pyo Kim of Kyung Hee University.

2.7.1. Reagents

HPLC-grade acetonitrile, chloroform, methanol, water, and isopropanol were purchased from J.T. Baker (Avantor Performance Material, PA, USA) and ammonium formate, acetic acid, and formic acid were purchased from Sigma-Aldrich (St. Louis, MO, USA).

Trimethylsilyldiazomethane (TMSD) was purchased from Tokyo Chemical Industry Co., Ltd. (Tokyo, Japan). Kyung Hee University team used the synthetic lipid standards as follows: TG (11:1–11:1–11:1), DG (8:0–8:0), MG (15:1), PA (10:0–10:0), PC (10:0–10:0), PE (10:0–10:0), PG (10:0–10:0), PI (8:0–8:0), PS (10:0–10:0), LPA (17:0), LPC (13:0), LPE (14:0), LPG (17:1), LPI (17:1), LPS (17:1), SM (d18:1–12:0), SO (d17:1), SO1P (d17:1), SA (d17:0), SA1P (d17:0), Cer (d18:1–12:0), Cer1P (d18:1–12:0), dCer (d18:0–12:0), dCer1P (d18:1–16:0), ChE (10:0), Cholesterol-d7 were purchased from Avanti Polar Lipids (Alabaster, AL, USA).

2.7.2. Lipid extraction

A two-step method was used for lipid extraction, including neutral, positive, and anionic (An et al., 2021; Breil et al., 2017). Each lipid standard was dissolved in chloroform and stored at −20 °C until use. It was diluted to the desired concentration using methanol. Plasma samples were placed in a microcentrifuge tube (1.5 ml). Next, 1 ml of chloroform/methanol (1:2; v/v) with internal standards (IS) was added and performed the incubation on ice for 10 min followed by vigorous vortexing and centrifugation (13,800 ×*g*, 2 min at 4 °C). The supernatant (900 μl) was transferred to a new microcentrifuge tube. Subsequently, 750 μl of chloroform/methanol/37 % hydrochloric acid (1 N HCl) (40:80:1, v/v/v) was added to the microcentrifuge tube and incubated at room temperature for 15 min, followed by 230 μl of cold chloroform and 430 μl of cold 0.1 N HCl were added to the samples, and the samples were vortexed and centrifugated (6500 ×*g*, 2 min at 4 °C). The organic phase at the bottom layer was collected and pooled with the first extracted lipid solution. The pooled extracted lipid samples were divided into two equal aliquots and dried with a SpeedVac concentrator (Hypercool, Labex, Republic of Korea). One aliquot was dissolved in 30 μl of solvent A for neutral and positive lipid analyses and the other was dissolved in 10 μl of methanol for the TMSD methylation reaction and anionic lipid analyses.

2.7.3. TMSD methylation

The TMSD methylation was used for analyzing anionic lipids that were difficult to analyze by LC-MS due to peak tailing. For TMSD methylation, an equal volume solution of 2 M TMSD in hexane was added to the lipid extract dissolved in 10 μl of methanol, and observed that the solution containing TMSD turned yellow. Next, the samples were vortexed for 30 s followed by incubation at 37 °C for 15 min. To terminate the methylation, glacial acetic acid was added to each sample. Finally, the samples with completed methylation turned colorless. These samples were subjected to subsequent LC-MS analysis (Lee et al., 2013; Lee et al., 2016).

2.7.4. Quantitative lipid analysis using LC-MS

HPLC-ESI-MS/MS analyses were performed on a triple quadrupole mass spectrometer (QQQ LC-MS 6490 series, Agilent Technologies) coupled to an Agilent 1290 infinity series HPLC instrument (Agilent Technologies, Santa Clara, CA, USA). The used column was a Hypersil GOLD column (2.1 × 100 mm ID; 1.9 μm, Thermo Science) and the temperatures of the autosampler tray and column oven were set to 4 °C and 40 °C, respectively. The mobile phase consisted of solvent A (methanol-acetonitrile-water, 19:19:2, v/v/v, 20 mM ammonium formate with 0.1 % (v/v) formic acid) and solvent B (isopropanol, 20 mM ammonium formate with 0.1 % (v/v) formic acid). The injection volume was 10 μl and the total run time was 33 min for each analysis. The LC gradient system was performed as follows: 0–5 min, 5 % solvent B; 5–15 min, 5–30 % solvent B; 15–22 min, 30–90 % solvent B; 22–27 min, 90 % solvent B; 27–28 min, 90–5 % solvent B; and 28–33 min, 5 % solvent B, at a constant flow rate of 0.25 ml/min.

The typical operating source conditions for lipid analysis in the positive ion ESI mode were as follows: 500 V of nozzle voltage, 4000 V positive mode of capillary voltage, and sheath gas flow of 11 l/min. The flow rate of the nitrogen drying gas was set at 13 l/min and the nebulizer was set at 40 psi. Gas and drying gas temperatures were maintained at 200 °C/180 °C for neutral and positive lipid analysis and at 180 °C/180 °C for TMSD-reacted lipid analysis (optimized condition). We targeted 27 lipid classes as follows: five neutral lipids [*Triacylglycerol (TG), Diacylglycerol (DG), monoacylglycerol (MG), cholesterylester (ChE), and cholesterol], six phospholipids [phosphatidic acid (PA), phosphatidylcholine (PC), phosphatidylethanolamine (PE), phosphatidylglycerol (PG), phosphatidylinositol (PI), and phosphatidylserine (PS)], six lysophospholipids [lysophosphatidic acid(LPA), lysophosphatidylcholine (LPC), lysophosphatidylethanolamine (LPE), lysophosphatidylglycerol (LPG), lysophosphatidylinositol (LPI), and lysophosphatidylserine (LPS)], and nine sphingolipids [sphinganine (SA), sphingomyelin (SM), sphingosine (SO), ceramide (Cer), dihydroceramide (dCer), ceramide-1-phosphate (Cer1P), dihydroceramide-1-phosphate (dCer1P), sphinganine-1-phosphate (SA1P), sphingosine-1-phosphate (SO1P)]*. Experiments were performed in the positive mode and we applied the dynamic multiple reaction monitoring (dMRM) approaches to analyze the target lipids in individual samples using the optimal MRM conditions, including MS/MS collision energy, computed transitions, and retention time (RT) for various lipid species. The MRM transition and MS/MS collision energy applied to the analysis were in Supplementary Table S1.

2.7.5. Data processing and statistical analysis of the dataset obtained using MRM

Identification and quantification of targeted lipids were performed using Agilent Mass Hunter Workstation Data Acquisition software. Qualitative Analysis B.06.00 software (Agilent Technologies, Wilmington, DE, USA) was used to export the *m/z* of precursor ions, m/z of product ions, and retention time (RT) of target lipids in the MRM data. Skyline software package (MacCoss Lab, University of Washington, Seattle, WA, USA) was used with an in-house database to calculate the peak area of each assigned lipid in the replicated raw data. Lipid abundance was normalized to the internal standard peak area and the differences between the groups were found to be significant via Student's *t*-test and the fold change was calculated using Microsoft Excel software. For the statistical analysis of the lipid dataset, including principal component analysis (PCA) plot, volcano plot, and hierarchical cluster analysis (HCA) were performed on MetaboAnalyst (www.metaboanalyst.ca).

2.8. Statistical analyses

Statistical analyses were performed using GraphPad Prism software (Version 8). ANOVA with Tukey's multiple comparison test and unpaired two-tailed *t*-tests were used. Each measurement was expressed as mean ± s.e.m. as stated in the figure legend.

3. Results

3.1. Vutiglabridin inhibits senescence in the GA muscle, eWAT, liver, kidney, and spleen

Vutiglabridin was fed to 20-month-old male mice at 50 mg/kg (mpk) mixed with the diet for 3 months to test its anti-ageing effects (VO: Vutiglabridin treated Old) (Fig. S1). As a non-treated control (NO: Normal Old), age-matched aged mice were fed a normal diet, and young mice (2 months old) were used as a young control (NY: Normal Young).

We performed the SA-β-gal assay in the GA muscle, eWAT, liver, kidney, and spleen to confirm the effects of vutiglabridin on senescence at the tissue level. The SA-β-gal activity in the spleen increased by 2.4 fold in the NO compared to the NY ($P = 0.0816$). When compared to NO, the SA-β-gal activity in the VO was reduced by 1.78 fold with vutiglabridin treatment ($P = 0.2165$). The difference was not statistically significant, but we did notice that one aged NO mouse had a significantly lower outlier than other mice in the same group (Fig. 1d). The NO significantly increased the SA-β-gal activity in the kidney by 2.7 fold

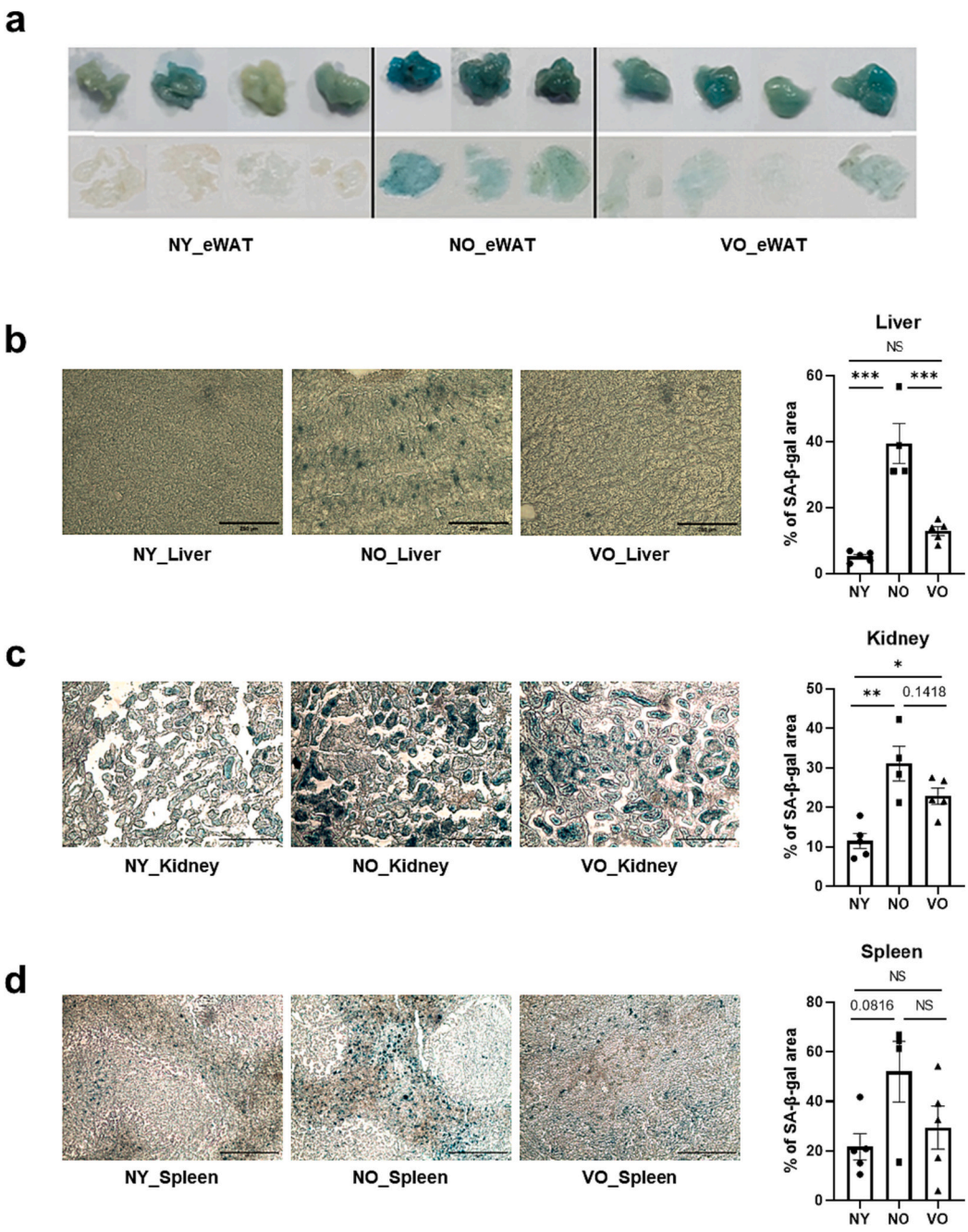

Fig. 1. Vutiglabridin decreases the SA-β-Gal activity in various tissues of aged mice. (a) eWAT depots SA-β-gal results. n of NY, NO, and VO were 3, 4, and 4, respectively; (b) Representative figure of liver SA-β-gal results. Scale bar = 250 μm (left) and quantification of SA-β-gal activity in the liver(right); (c) Representative figure of kidney SA-β-gal results. Scale bar = 500 μm (left) and quantification of SA-β-gal activity in the kidney (right); (d) Representative figure of spleen SA-β-gal results. Scale bar = 250 μm (left) and quantification of SA-β-gal activity in the spleen (right). Each activity is represented as the average value of five different photos in random locations. n of NY, NO, and VO were 5, 4, and 5, respectively. Error bars show mean ± s.e.m. NS, not significant; $*P < 0.05$, $**P < 0.01$, $***P < 0.001$. One-way ANOVA followed by Tukey's multiple comparisons tests.

when compared to the NY. When compared to NO, the SA-β-gal activity in the VO was reduced by 1.36 fold with vutiglabridin treatment ($P = 0.1418$) (Fig. 1c). The activity of SA-β-gal staining in the liver was increased approximately 7-fold in NO compared to NY. The SA-β-gal activity was significantly reduced with vutiglabridin treatment (Fig. 1b). The SA-β-gal staining was reduced in the VO in eWAT compared to NO (Fig. 1a). These findings suggest that vutiglabridin may have anti-ageing properties.

qPCR was performed to confirm whether SASP and senescence-associated genes such as *Cdkn1a (p21), Cdkn2a (p16), Cxcl2, Il-6, J-chain, Sparc, Klotho,* and *Ppar-γ* expression were altered in aged mice. The expression level of *Cdkn1a, Cdkn2a, Cxcl2, Il-6,* and *J-chain* that were significantly increased with ageing in the spleen were significantly decreased in the VO compared to NO (Fig. 2e). The *Cdkn2a* expression in the GA muscle, which had significantly increased with ageing, was reduced in the VO compared to NO ($P = 0.0513$). The *Il-6* expression, which increased with age, was significantly reduced in VO compared to NO, though the difference in expression was not significant ($P = 0.1452$). We also found that the *Cxcl2* expression increased with age and was lower in VO compared to NO ($P = 0.1112$), though this was not statistically significant. The *Sparc* expression in the VO was found to be lower than in the NO, but this was not statistically significant (Fig. 2a). The expression level of *Cdkn1a, Cdkn2a, Cxcl2, Il-6, Klotho*, and *Ppar-γ* in the kidney was not significantly altered with ageing, and there were no differences in VO compared to NO. However, when one outlier was removed from the VO, we discovered that the *Cdkn2a* expression was slightly reduced compared to NO. We also found that *Klotho* and *Ppar-γ* were slightly altered in the VO when compared to NO, though the differences were not statistically significant. The *J-chain* expression was significantly upregulated with ageing in the VO but downregulated in the NO ($P < 0.0768$) (Fig. 2d). The *Cdkn2a* expression in the liver, which increased with age, significantly reduced VO. Although *Cxcl2* levels

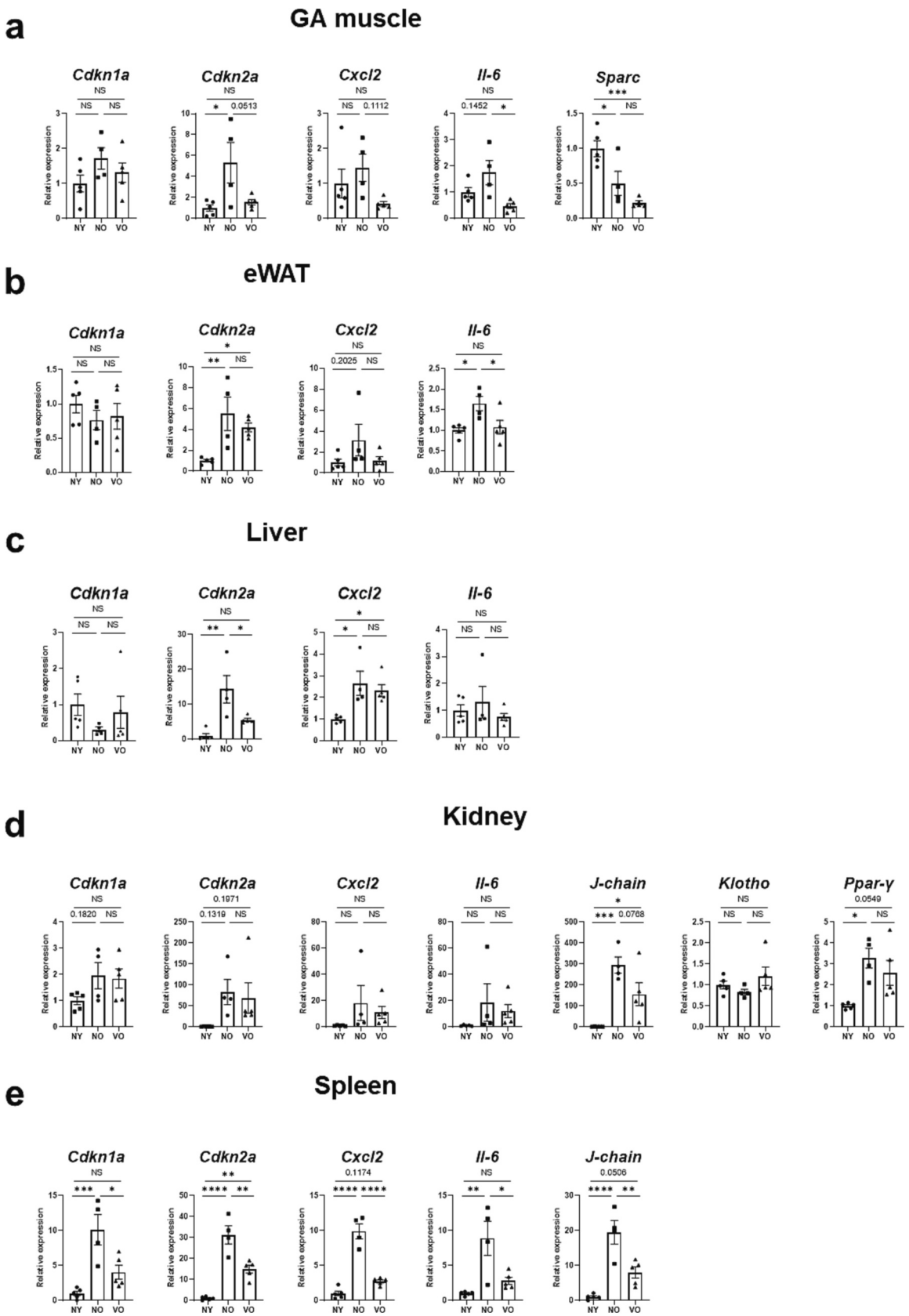

Fig. 2. Vutiglabridin ameliorates SASP and senescence-associated gene expressions in the various tissues of aged mice. (a) Relative *Cdkn1a*, *Cdkn2a*, *Cxcl2*, *Il-6*, *Spacr* mRNA level in the GA muscle; (b) Relative *Cdkn1a*, *Cdkn2a*, *Cxcl2*, *Il-6* mRNA level in the eWAT; (c) Relative *Cdkn1a*, *Cdkn2a*, *Cxcl2*, *Il-6* mRNA level in the liver; (d) Relative *Cdkn1a*, *Cdkn2a*, *Cxcl2*, *Il-6*, *J-chain*, *Klotho*, and *Ppar-γ* mRNA levels in the kidney; (e) Relative *Cdkn1a*, *Cdkn2a*, *Cxcl2*, *Il-6*, *J-chain* mRNA level in the spleen. Each result is normalized by the NY. n of NY, NO, and VO were 5, 4, and 5, respectively. Data are mean ± s.e.m. NS, not significant; $^{*}P < 0.05$, $^{**}P < 0.01$, $^{***}P < 0.001$. One-way ANOVA followed by Tukey's multiple comparisons tests.

increased with age, there was no difference in NO or VO levels. We discovered expression patterns that differed from those previously observed in *Cdkn1a*. The *Cdkn1a* expression was lower in NO compared to NY, but the difference was not statistically significant. The expression levels of *Il-6* were not different between the three groups (Fig. 2c). In eWAT, the *Il-6* expression significantly increased with ageing while NO decreased. The *Cdkn2a* expression levels in NO increased significantly when compared to NY. Although not statistically significant, we found a decrease in the *Cdkn2a* expression in VO compared to NO. The *Cxcl2* expression levels increased with age and decreased with VO. The *Cdkn1a* expression, on the other hand, remained unchanged (Fig. 2b). Although the *Cdkn2a* expression was significantly higher in the NO liver and eWAT compared to NY, the expression of *Cdkn1a*, one of the widely used senescence markers, was lower in the NO liver and there was no difference in eWAT.

According to a previous study using the IMR 90 cell line, *Cdkn1a* is required for cell cycle arrest in the early stages of senescence but rapidly decreases, whereas *Cdkn2a* increases in the late stages of senescence. *Cdkn2a* is required for late-stage senescent cell cycle arrest, and increased *Cdkn2a* was associated with increased SA-β-gal activity (Stein et al., 1999). These findings suggest that NO eWAT, liver, kidney, and spleen cells are in the late stages of senescence, and when combined with the SA-β-gal activity findings, VO may not have reached this stage yet. As a result, we expect vutiglabridin to slow the ageing process.

3.2. Vutiglabridin improves muscle homeostasis in the GA muscle

We used bulk RNA sequencing (RNA-seq) on the GA muscle to gain a better understanding of the effects of vutiglabridin on ageing. We sorted genes under each sorting condition of categories to determine the tendency of vutiglabridin effects (Fig. S2a and b). Following that, we used gene ontology analysis to look into how vutiglabridin affects signalling pathways. We discovered that vutiglabridin altered the organisation of the external encapsulating structure, cellular component biogenesis, superoxide anion generation, and RNA processing (Fig. 3a). These findings suggested that GO analysis data could be linked to ECM, mitochondrial biogenesis, ROS, and RNA splicing.

ECM-related GO pathways were commonly represented in the GO analysis data, including collagen fibril organisation, external encapsulating structure organisation, extracellular structure organisation, extracellular matrix organisation, cell adhesion, signalling regulation, cell communication regulation, and signalling transduction regulation (Fig. 3a). The main components of ECM, collagens and fibronectins, are involved in signalling pathways to the cellular response by various receptors such as integrin and DDR (Heino, 2014; Leitinger, 2014). First, we looked at the gene expressions of collagen, fibronectin, integrin, and discoidin domain receptor (DDR) to see if there was a link between the GO analysis results and muscle ageing under these three conditions: 1) Common genes with $P < 0.1$ in the NO_VO and $P < 0.1$ in the NO_NY, 2) Genes with similar patterns in NY and VO, but not in NO, and 3) Prominently changed genes in only VO. There were many changes in gene expression of the collagen IV family, collagen VI family, fibronectin, and their related signal receptors such as *Itga1*, *Itga11*, *Itgb1*, and *Ddr2* in the VO compared to NO (Fig. 3b and c) (Zeltz and Gullberg, 2016).

Muscle ageing may alter the ECM environment, which may affect muscle regeneration capacity (Yamakawa et al., 2020) and satellite cell activity and function (Muñoz-Cánoves et al., 2020). Satellite cells are required for muscle homeostasis, including muscle regeneration capacity, and their activity and function can be altered by ECM remodelling during ageing (Muñoz-Cánoves et al., 2020). When VO was compared to NO, the gene expression of the muscle regeneration-related gene set changed (Muñoz-Cánoves et al., 2020). The gene expressions of muscle regeneration were also altered by vutiglabridin when we sorted the genes using the mouse genome informatics (MGI) database (Fig. 3d). When compared to NO, the expression of satellite cell-related genes (Pallafacchina et al., 2010) in the VO tended to be regulated similarly with the NY (Fig. 3e). Furthermore, except for the expression of *Myog*, the expressions of the *Myod* family, which is an important myogenic regulatory factor (MRF) (Buckingham and Rigby, 2014), tended to be modulated similarly with the NY in the VO as compared to NO (Fig. 3f). These findings suggest that vutiglabridin may improve satellite cell function-related gene expression by regulating the expression of ECM-related genes.

Following that, we searched the literature on muscle ageing and satellite cell function for specific mechanisms by which vutiglabridin could affect the expression of satellite cell function-related genes. We discovered the FGF family, which is essential for satellite cell self-renewal and skeletal muscle repair (Pawlikowski et al., 2017). When compared to NO, gene expression of the FGF family, including *Fgf5*, *Fgf6*, *Fgf11*, and *Fgf13*, tended to be modulated in a direction similar to NY in the VO. Furthermore, when compared to other groups, the expression of *Fgf9* was significantly higher in VO (Fig. 3g and h). According to previous studies, increasing FGF2 causes stem cell exhaustion (López-Otín et al., 2013). The *Fgf6* overexpression improves systemic metabolism and increases muscle weight and function in high-fat diet (HFD) mice (Xu et al., 2021). In ischemia-reperfusion (IR) models, FGF9 promotes angiogenesis, muscle regeneration, and muscle function, which occurs during peripheral arterial disease (PAD) (Frontini et al., 2011), which is primarily caused by ageing (Paradis et al., 2019). The FGF family regulates satellite cell proliferation via ERK (Pawlikowski et al., 2017) and JNK (Wu et al., 2020), as well as satellite cell activation and differentiation via p38 (Pawlikowski et al., 2017). Next, we looked into how vutiglabridin affected the expression of FGF signalling pathways and genes involved in satellite cell function. When compared to NO, the gene expression of serial signalling pathways such as *Hspg2*, *Fn1*, *Itgb1*, *Frs2*, *Grb2*, *Sos*, *Hras*, *Kras*, *Ptpn11*, *Raf*, *Map2k1*, *Spry2*, and *Dusp6* tended to change in a direction similar to NY (Fig. 3g) (Xie et al., 2020). Finally, while the expression of *Mapk1* and *Mapk8* increased with age, it decreased with NY in the VO. Nonetheless, the expression of *Mapk14* was not changed in the VO (Fig. 3g and h). These findings supported previous research that satellite cells prefer quiescence in a young niche while promoting stem cell activation and differentiation in an old niche (Yamakawa et al., 2020). In other words, vutiglabridin may regulate satellite cell state-related genes to induce satellite cell quiescence to retain satellite cell function rather than activation and differentiation and promote muscle homeostasis.

Matrix remodelling enzymes such as MMPs, TIMPs, adamalysins, and meprins have the potential to alter the ECM environment (Leitinger, 2014). ROS can both directly and indirectly regulate the expression of matrix remodelling enzymes (Moon et al., 2004; Alcazar et al., 2007; Gomes et al., 2012). ECM has the potential to influence oxidative stress (Martins et al., 2021) and mitochondrial morphology (Chen et al., 2021). Furthermore, GO analysis data suggest that vutiglabridin reduced superoxide anion generation while increasing cellular component biogenesis (Fig. 3a). As a result, we hypothesize that vutiglabridin alters the expression of ECM environment-related genes by decreasing the expression of ROS-related genes while increasing the expression of mitochondria biogenesis-related genes. As expected, the various gene expressions of many matrix remodelling enzymes that changed with ageing improved in the VO compared to NO, including MMP, TIMP, ADAMTS, and ADAM (Fig. 3i and j). Furthermore, when compared to NO, the gene expressions of SASP (*Tnf* (Moon et al., 2004), *Tgf1* (Gomes et al., 2012)), mitochondrial fusion (*Mfn1*, *Mfn2*, and *Opa1*), and fission (*Dnm1l*) (Westermann, 2010) were modulated in the VO (Fig. 3k and l). These findings suggested that vutiglabridin may regulate the expression of satellite cell function-related genes by restoring gene expressions involved in ECM homeostasis in aged mice's GA muscles. Vutiglabridin, when taken together, may improve muscle homeostasis by regulating the expression of ECM environment-related genes in the GA muscle of aged mice.

a

Category 1. Up-regulation

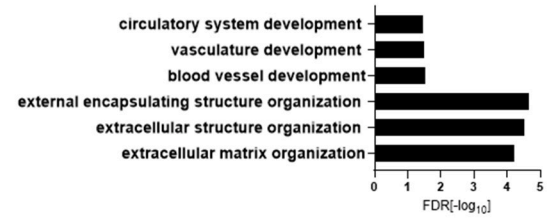

Fold Enrichment
8.15
11.34
11.98
27.4
27.5
27.59

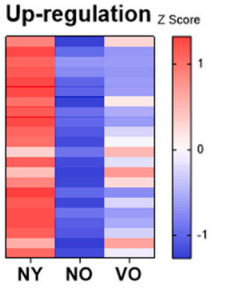

Category 2. Up-regulation

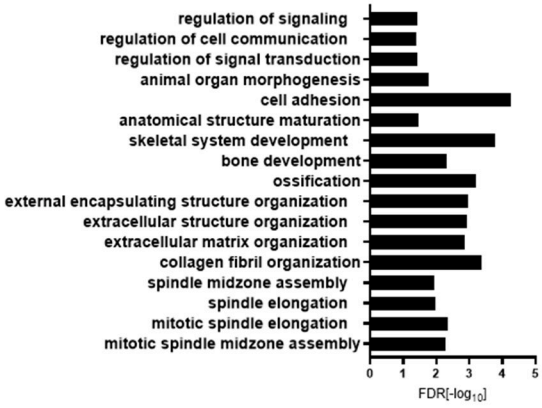

Fold Enrichment
1.75
1.75
1.81
2.61
3.61
4.75
4.45
5.64
6.07
5.51
5.53
5.55
16.38
40.2
40.2
55.27
55.27

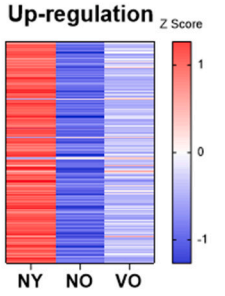

Category 4. Down-regulation

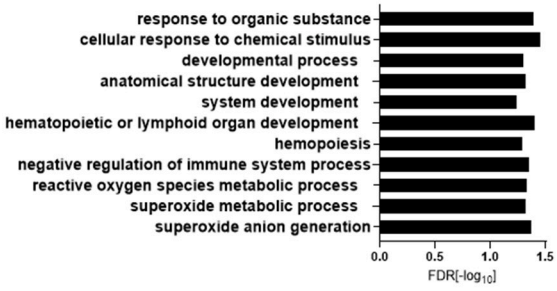

Fold Enrichment
2.39
2.51
1.82
1.86
2.09
3.93
4.23
5.21
14.08
26.13
48.35

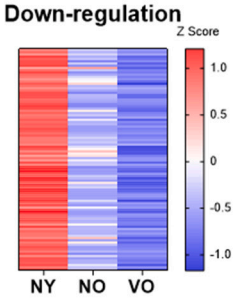

Category 5. Up-regluation

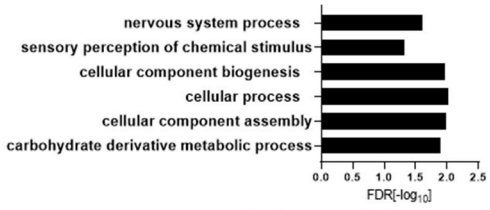

Fold Enrichment
0.25
0.07
2.01
1.2
2.02
2.68

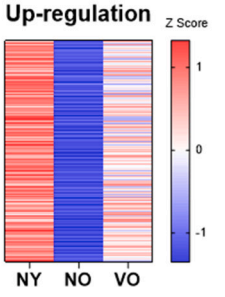

Category 5. Down-regulation

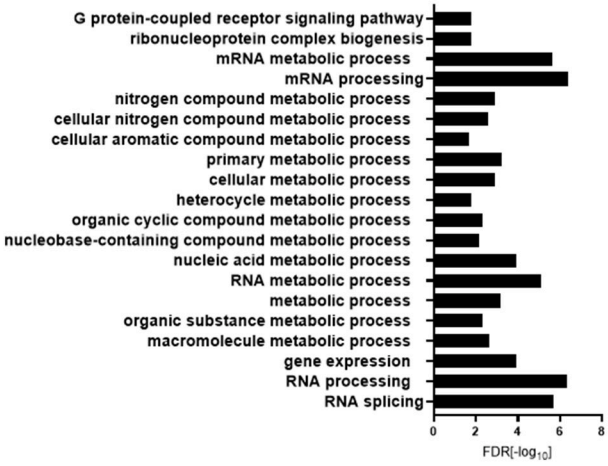

Fold Enrichment
0.12
3.97
4.72
5.94
1.59
1.9
1.88
1.58
1.59
1.93
1.92
2.00
2.45
3.00
1.5
1.47
1.6
2.27
4.32
6.41

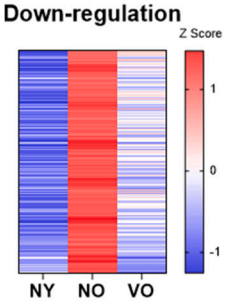

Fig. 3. Vutiglabridin improves muscle homeostasis in the GA muscle of aged mice. (a) Biological processes (BP) with gene expressions by category; (b) The heatmap of the differentially expressed genes by the collagen, and fibronectin with *z*-score; (c) The heatmap of the differentially expressed genes by the integrin, DDR with *z*-score; (d) The heatmap of the differentially expressed genes by the muscle regeneration pathways with *z*-score; (e) The heatmap of the differentially expressed genes by the satellite cell related to pathways with *z*-score; (f) Relative expression of each gene, *Myf5*, *Myf6*, *Myod1*, and *Myog* respectively by RNA seq; (g) The heatmap of the differentially expressed genes by FGF signalling pathways with z-score; (h) Relative expression of each gene, *Fgf2*, *Fgf5*, *Fgf6*, *Fgf9*, *Fgf11*, *Fgf13*, *Mapk1*, *Mapk8*, *and Mapk14*, respectively by RNA seq; (i) The heatmap of the differentially expressed genes by ECM remodelling enzymes with z-score; (j) Relative expression of each gene, *Mmp2*, *Mmp9*, *Mmp14*, *Mmp15*, *Mmp19*, *Timp2*, *Timp3*, and *Timp4,* respectively by RNA seq; (k) The heatmap of the differentially expressed genes by *SASP* & mitochondria morphology with z-score; (l) Relative expression of each gene, *Tgfb1*, *Dnm1l*, *Mfn1*, and *Mfn2* respectively by RNA seq. n of NY, NO, and VO were 5, 4, and 5, respectively. Data are mean ± s.e.m. NS, not significant; $^{*}P < 0.05$, $^{**}P < 0.01$, $^{***}P < 0.001$. Unpaired two-tailed *t*-test.

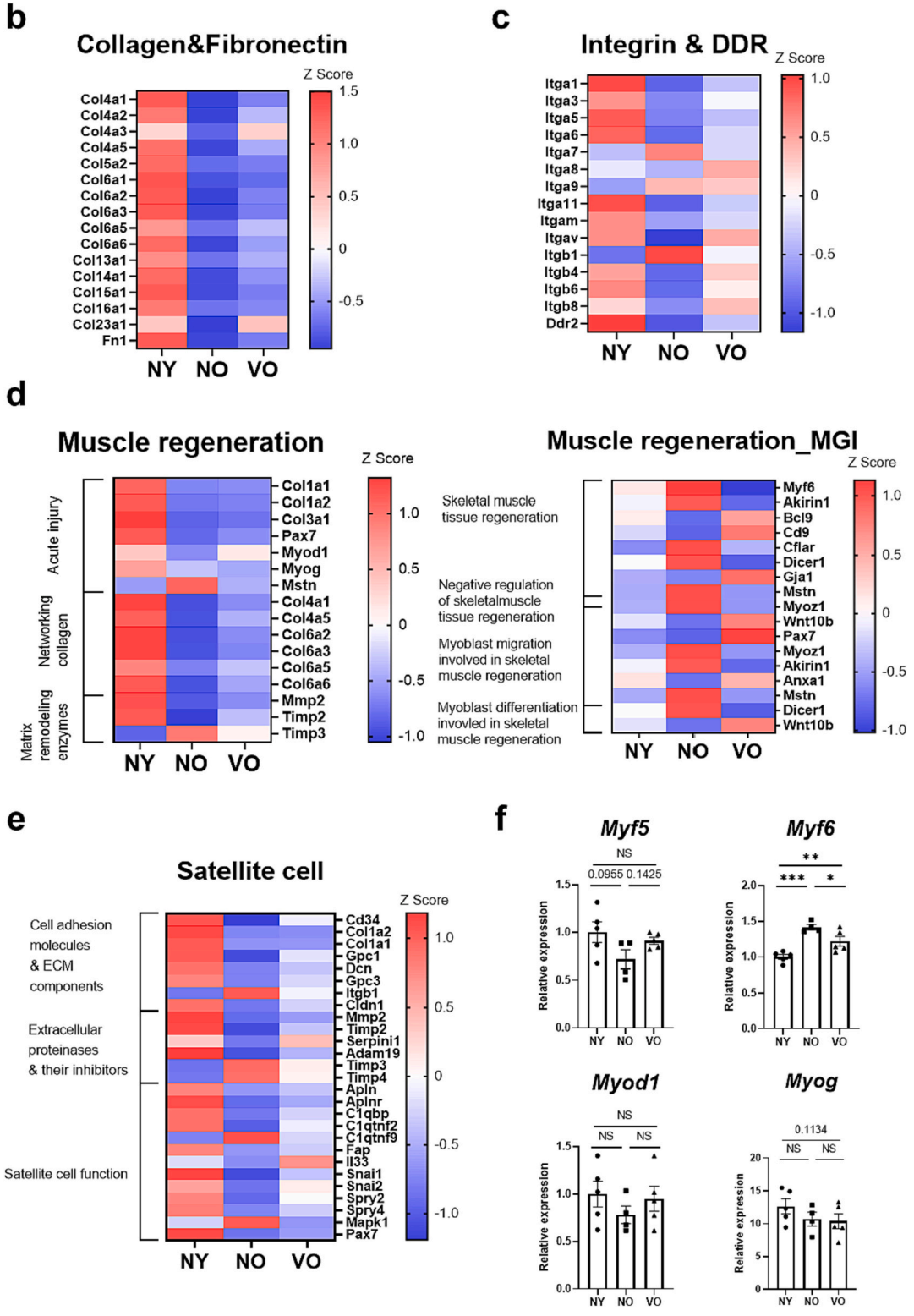

Fig. 3. (*continued*).

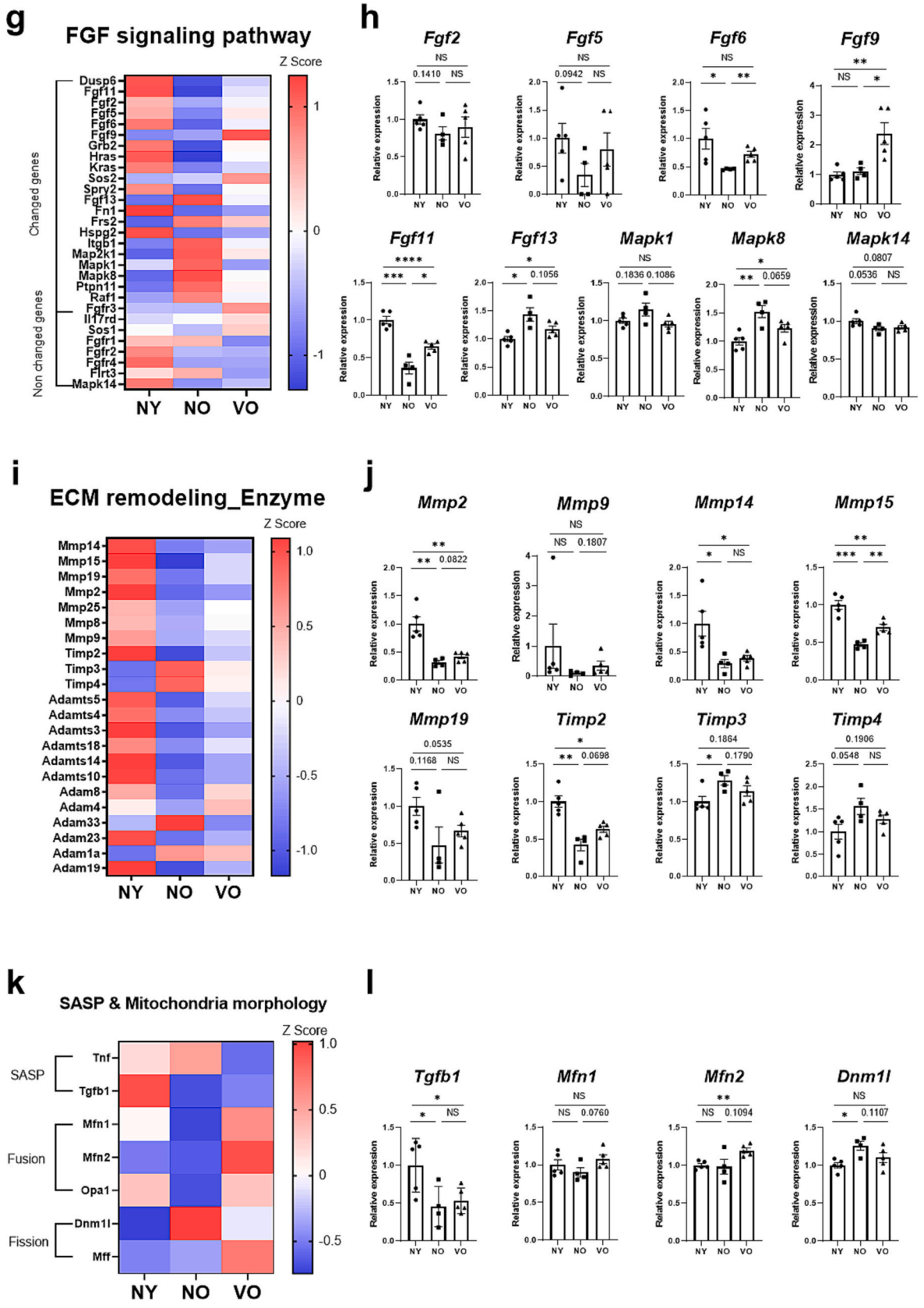

Fig. 3. (*continued*).

3.3. Vutiglabridin restores insulin sensitivity in the eWAT

RNA-sequencing in the liver and eWAT was performed to determine the mechanism by which vutiglabridin affects anti-ageing. The expression of genes that changed significantly with ageing (p-value < 0.05) but were alleviated by vutiglabridin treatment was sorted, as few genes changed significantly in VO when compared to NO. As previously mentioned in the qPCR data, these few changes were thought to be caused by vutiglabridin delaying the ageing process. As a result, in eWAT, 752 genes increased in ageing (up-differentially expressed genes (DEGs)) and 892 genes decreased in ageing (down-DEGs). Using sorted genes, gene ontology (GO) analysis was performed, and vutiglabridin effects were identified using the top 16 and top 6 enriched biological processes (BPs), respectively.

Only the highest process was chosen to investigate the various effects of vutiglabridin on ageing, and relative gene expression of up or down GO-associated genes was indicated using a heatmap (Fig. 4a top). In the up-regulated GOs with ageing, there was retinoic acid-inducible gene-1 (RIG-1) and p38-MAPK signalling (Fig. 4a top). We next focused on NF-κB signalling because RIG-1 and p38-MAPK signalling can be activated by environmental stress such as ROS, inflammation, and DNA damage, and can stimulate NF-κB signalling, which stimulates SASP secretions such as IL-6 (Salminen et al., 2012). IκB/NF-κB signalling was one of the up-regulated GOs, consistent with the increase in these signallings, and this result was consistent with the qPCR result of *Il-6* expression in eWAT (Fig. 2b). These findings suggest that vutiglabridin treatment may reduce chronic inflammation that has increased with age.

We then looked to see if insulin resistance appeared because p38-MAPK signalling suppresses glucose transporter-4 (GLUT4) expression, which causes insulin resistance and hyperglycemia (Wu et al., 2009). When treated with vutiglabridin, the expression of *Slc2a4*, which encodes GLUT4, was found to be higher in NO compared to NY (Fig. 4b). The endoplasmic reticulum unfolded protein response (UPR) was one of the up-regulated GOs, and protein folding was one of the down-regulated GOs (Fig. 4a). Chronic ER stress is caused by unfolded protein phosphorylates JNK, which causes IRS-1 phosphorylation, which inhibits insulin receptor signalling. Insulin resistance is caused by impaired insulin signalling (Amen et al., 2019). As a result, we confirmed the *Jnk* expression. The mRNA level of JNK, known as MAPK8, increased with age but was significantly reduced by vutiglabridin treatment (Fig. 4c). These findings suggest that insulin resistance may occur in NO eWAT but not in VO.

Dynein mediates autophagosome centripetal trafficking (Kimura et al., 2008), and autophagosome-lysosome fusion occurs primarily in the perinuclear (Zaarur et al., 2014). According to a recent study, the relocation of autophagosomes and lysosomes to the perinuclear region decreases with age, resulting in decreased fusion efficiency and subsequent degradation of the sequestered cargo (Bejarano et al., 2018). As a result, we hypothesised that the increase in ER stress was caused by a decrease in outer dynein arm assembly, which decreased GO in NO eWAT (Fig. 4a bottom).

In obese mice, hepatic *EphB4* overexpression reduces InsR and increases hepatic and systemic insulin resistance, whereas *EphB4* inhibition improves insulin resistance and glucose intolerance (Liu et al., 2022). Furthermore, *EphB4* expression was significantly lower in VO eWAT compared to NO, indicating increased insulin sensitivity (Fig. 4d).

Thus, these findings suggest that vutiglabridin treatment-induced increased *Slc2a4* expression and improved insulin receptor signalling may alleviate insulin resistance in aged eWAT.

3.4. Vutiglabridin prevents FALC-induced inflammation in eWAT

Fat-associated lymphoid clusters (FALCs) were found to be more prevalent in visceral adipose tissue (VAT) with ageing (Lumeng et al., 2011). The NLRP3 inflammasome is required for the formation of aged FALCs and aged adipose B cells (AABs). In VAT, IL-1 signalling increased FALCs while decreasing insulin sensitivity (Camell et al., 2019). The next step was to see if vutiglabridin treatment affected FALC. When compared to NY, *Nlrp3* expression appeared to moderately increase in NO and was reduced by vutiglabridin treatment (Fig. 4e). One of the up-regulated GOs was IL-1 signalling activated by NLRP3 to expand FALC (Fig. 4a top). SIRT2 deacetylates NLRP3 to inactivate it, and its expression decreases with age, according to a recent study. SIRT2 prevents and reverses inflammation and insulin resistance associated with ageing (He et al., 2020). As a result, we assessed the level of *Sirt2* expression in each group. The *Sirt2* expression was significantly lower in NO than in NY, but this was alleviated by vutiglabridin treatment (Fig. 4f). These findings suggest that vutiglabridin treatment may reduce the NLRP3 inflammasome, which causes FALC.

The *J-chain* expression, which indicates B-cells, increased with age, but there were no differences between NO and VO (Fig. 4g). As 'T cell differentiation involved in immune response' and 'CD4-positive, alpha-beta T cell activation' appeared in GO increased in NO, T cells polarised to a pro-inflammatory phenotype that secreted type 1 cytokines such as TNF-α and IL-6 were increased with ageing (Fig. 4a top). This increase in pro-inflammatory T cells correlated with *Il-6* expression (Fig. 2b). Monocyte-derived macrophages accumulated with age due to CCL2-CCR2 interaction and loss of CCR2 expression when activated (Chini et al., 2020; Heymann and Tacke, 2016). In NO, the *Ccl2* expression increased significantly while *Ccr2* expression decreased (Fig. 4h). These findings suggest that CCR2+ blood monocytes were accumulated in eWAT by increased *Ccl2* expression, and that these monocytes differentiated and activated into macrophages as the *Ccr2* expression was reduced.

M1 macrophages were found to be more prevalent in aged WAT, and CD38 is one of the M1 markers (Jablonski et al., 2015). Senescent cells and their SASP promote the accumulation of $CD38^+$ macrophages in WAT (Covarrubias et al., 2020; Chini et al., 2020). The *Cd38* expression was higher in NO than in NY and was reduced by vutiglabridin treatment (Fig. 4i). The *Cd86* expression, another M1 macrophage marker (Liu et al., 2020), was examined. The *Cd86* expression pattern matched the *Cd38* expression pattern (Fig. 4i). In addition, vutiglabridin treatment reduced some chemokine expression that increased with age (Fig. 4h).

These findings suggest that vutiglabridin can regulate pro-inflammatory T cells and monocyte recruitment, both of which increase inflammation, while having no effect on B cells. As a result, vutiglabridin may be able to prevent FALC-induced inflammation in eWAT.

3.5. Vutiglabridin improves NAD^+ metabolism in eWAT

According to recent research, CD38 can act as an ectoenzyme to convert nicotinamide mononucleotide (NMN), the precursor of NAD^+, into nicotinamide (NAM) (Covarrubias et al., 2020; Chini et al., 2020). As a result, increased *Cd38* expression may lower NMN levels, impairing NO eWAT metabolism. As a result, we looked into whether NAD^+ metabolism was altered in NO eWAT. According to GO findings, the nicotinamide nucleotide metabolic pathway was down-regulated in NO (Fig. 4a bottom). The *Nampt* expression, a key enzyme in the NAD^+ recovery pathway (Covarrubias et al., 2021), was reduced in NO eWAT. Other NAD^+ metabolism enzymes, such as *Naprt* and *Oprt*, were reduced in NO when compared to NY, but this was mitigated by vutiglabridin treatment (Fig. 4k). Mice lacking adipocyte-specific NAMPT have lower NAD^+ levels in adipose tissue, increased insulin resistance, and metabolic dysfunction (Stromsdorfer et al., 2016). Other GOs that have been found to be down-regulated in eWAT include the 'carboxylic acid catabolic process' and 'generation of precursor metabolites and energy' (Fig. 4a bottom).

These findings suggest that vutiglabridin may improve NAD^+ metabolism and metabolic dysfunction in aged eWAT.

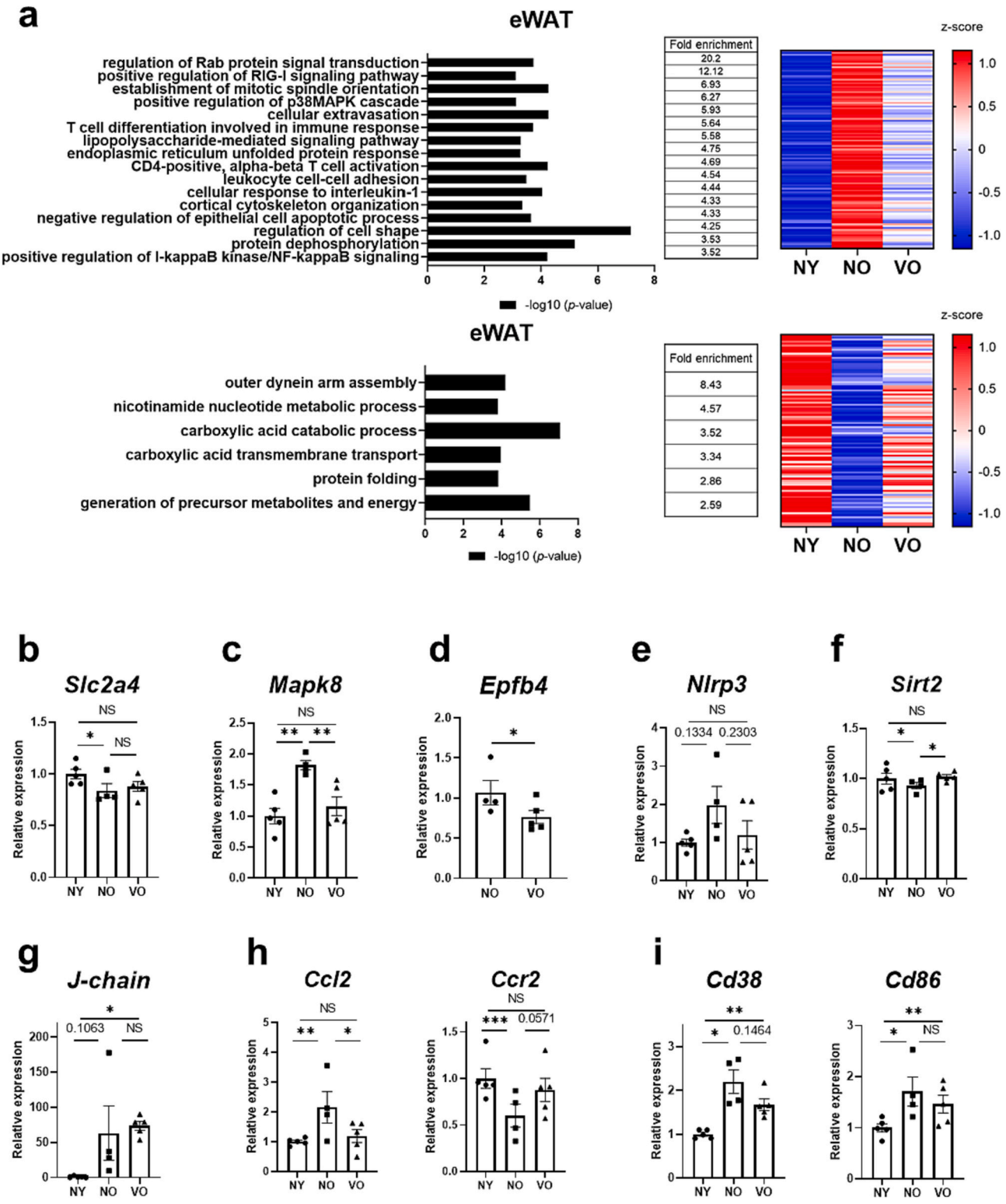

Fig. 4. Vutiglabridin alleviates metabolism and inflammageing in aged eWAT. (a) Top; Biological processes (BP) for genes that were up-regulated with ageing but were alleviated by vutiglabridin treatment in eWAT (right). Heatmap represents the expression levels of genes belonging to the biological processes (left). Bottom; Biological processes (BP) for genes that were down-regulated with ageing but were alleviated by vutiglabridin treatment in eWAT (right). Heatmap represents the expression levels of genes belonging to the biological processes (left). a, Expression was normalized by NY; (b–f) Relative expression of each gene, *Slc2a4*, *Mapk8*, *Epfb4*, *Nlrp3*, and *Sirt2* respectively; (g) Relative expression of *J-chain* in qPCR results; (h) Relative expression of *Ccl2* and *Ccr2*; (i) Relative expression of *Cd38* and *Cd86,* respectively; (j) Relative expression of *Ccl7*, *Ccl8*, *Ccl12*, *Ccl3*, and *Ccl7*; (k) Relative expression of *Nampt*, *Qprt*, and *Naprt*. n of NY, NO, and VO was 5, 4, and 5,

respectively. Data are mean ± s.e.m., NS, not significant; *$P < 0.05$, **$P < 0.01$, ***$P < 0.001$. An unpaired two-tailed *t*-test was performed in c-g, and i-l. One-way ANOVA followed by Tukey's multiple comparisons test was performed in h.

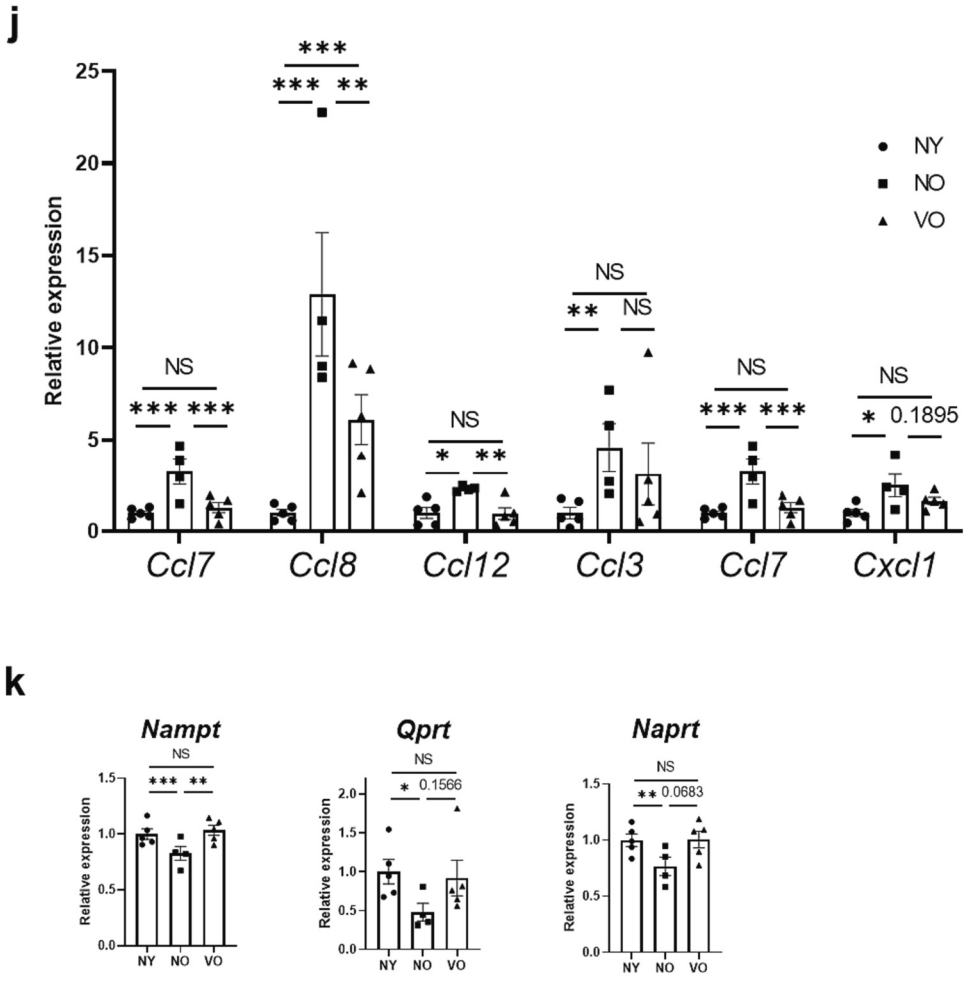

Fig. 4. (*continued*).

3.6. *Vutiglabridin reduces inflammation in the aged liver by preventing TLO formation*

Using the same criteria as eWAT, 699 genes that increased with age (up-DEGs) and 703 genes that decreased with age (down-DEGs) were chosen in the liver. We examined GO and identified vutiglabridin effects using the top 17 and 12 enriched BPs, respectively, and relative gene expression of up or down GO-associated genes was indicated using a heatmap (Fig. 5a). We started with immune-associated GOs in the liver because 9 of the 17 up GOs were immune-associated (Fig. 5a top). These up-regulated GOs suggest that chronic inflammation may occur in the NO liver. Various immune cells, including innate and adaptive immune cells, infiltrate chronically inflamed tissues. Tertiary lymphoid organs (TLO) are frequently organised by these cellular elements. This lymphocyte neogenesis is a dynamic process that begins with sparse lymphocyte infiltration and progresses to aggregates organised in secondary B-cell follicles with germinal centers (GC) and distinct T-cell regions containing DCs and high endothelial venules (HEV) (Aloisi and Pujol-Borrell, 2006). There were 'macrophage colony-stimulating factor signalling pathways, regulation of germinal center formation', and 'regulation of B cell proliferation' in up-regulated BPs (Fig. 5a top).

Endogenous molecules known as damage-associated molecular patterns (DAMPs) can cause inflammation. DAMPs are released during cellular stress and necrosis, and their levels rise with age. And DAMPs cause inflammation by activating pattern recognition receptors (PRRs) such as Toll-like receptors (TLRs) (Gong et al., 2020; Royce et al., 2019). TLR expression levels were then measured to confirm whether DAMPs were one of the causes of this inflammation. TLRs expression was higher in NO than in NY, but it was reduced by vutiglabridin treatment (Fig. 5b). In line with these increased TLR expressions, one of the up-regulated GOs was the 'MyD88-dependent toll-like receptor signalling pathway' (Fig. 5a top). The expression of *Pkn1, H2-DMa, Tnfaip3,* and *Tnfsf13b* were significantly increased in NO compared to NY, but this was alleviated by vutiglabridin treatment (Fig. 5c).

When NO was compared to NY, genes regulating lymphocyte homing and compartmentalization (Aloisi and Pujol-Borrell, 2006) were altered (Fig. 5d). Although lymphocyte homing and compartmentalization genes were increased in the VO liver compared to the NY liver, GC formation genes were not changed (Fig. 5d). As the expression of *Ccl2* and *Ccr2* increased in the NO liver compared to the NY liver, monocyte-derived macrophages accumulated (Fig. 5e). The M1 macrophage marker CD80 (Yunna et al., 2020) was significantly higher in the NO liver compared to the NY liver and slightly lower in the VO liver compared to the NO liver (Fig. 5f). As an immune response, M1 macrophages produce reactive oxygen species (ROS) and nitrogen oxide (NO) (Covarrubias et al., 2013), and monocytes were polarised into M1 macrophages under inflammatory conditions. In line with these findings, the up-regulated GO displayed two BPs: 'positive regulation of superoxide anion generation' and 'regulation of nitric oxide biosynthetic process' (Fig. 5a top).

These findings suggest that proinflammatory M1 macrophages accumulated in the NO liver, whereas anti-inflammatory M2 macrophages (Yunna et al., 2020) accumulated in the VO liver (Fig. 5f and g). Furthermore, the 'regulation of the interleukin-1 beta production pathway' increased in NO but not in VO (Fig. 5a top). As a result, these findings could imply that vutiglabridin treatment reduces chronic inflammation in the aged liver by preventing TLO formation.

3.7. Vutiglabridin enables mitochondria to function normally by allowing intact assembly of mitochondrial complex I

'Mitochondrial respiratory chain complex I assembly' was found in the down-regulated GOs (Fig. 5a bottom). This finding corroborated previous findings that mitochondrial enzymes, including complexes I and IV, were reduced in the aged liver (Navarro and Boveris, 2004). It has been reported that disrupting complex I assembly by reducing membrane subunit expression increases mitochondrial peroxide production. Without proton pumping or electron transport, incompletely assembled matrix subunits generate mitochondrial superoxide, reducing ETC efficiency and increasing ROS output (Miwa et al., 2014). According to this study, the GSH/GSSG ratio was higher in the VO liver compared to the NO liver (Fig. 5h), indicating less oxidative stress. However, the GSH/GSSG ratio did not show any significant differences in the VO spleen and kidney when compared to the NO spleen and kidney (Figs. S3a and b). Furthermore, mitochondrial complex I membrane subunits such as *Ndufa5* and *Ndufb2* were significantly lower in the NO liver compared to the NY liver but increased in the VO liver (Fig. 5i).

As a result of these findings, vutiglabridin treatment may restore mitochondrial complex I assembly, which reduces mitochondrial ROS formation.

3.8. Vutiglabridin alleviates ageing-related lipid profile changes

Because lipid profiles change with age (Montoliu et al., 2014) and vutiglabridin was thought to improve metabolism, we used LC-MS to see if vutiglabridin treatment changed the lipid profile. The principal component analysis (PCA) revealed that the NY, NO, and VO lipid profiles clustered differently (Fig. 6a). Fig. 6b depicts the overall changes in lipid composition. Ceramides have been found to accumulate in old worms and humans, and a ceramide-rich diet reduces the lifespan of *C. elegans* (Papsdorf and Brunet, 2019). Serum ceramide levels were linked to an increased risk of dementia/ Alzheimer's disease (Huang et al., 2014).

Ceramide accumulation promotes the development of age-related diseases. Reduced ceramide levels also slow the ageing process by increasing autophagy, decreasing ROS, carbon remodelling, energy metabolism, stress resistance, and genomic stability and extending lifespan. Ceramide accumulation and clustering in the plasma membrane prevent autophagosomes from fusing with lysosomes, reducing autophagic flux and promoting senescence (Huang et al., 2014). As a result, the ceramide levels were established. Ceramide levels rose with age and fell with vutiglabridin treatment (Fig. 6c). Ceramide accumulation is associated with increased oxidative stress and insulin resistance (Huang et al., 2014), which is consistent with the results of RNA-sequencing-based insulin resistance in eWAT.

S-adenosyl methionine (SAM) is required for the methylation of phosphatidylethanolamines (PEs) to generate phosphatidylcholines (PCs), and mice lacking phospholipid methylation have increased histone methylation, including H3K4me3, H3K36me3, and H3K79me3. This could be because when lipid methylation fails, more SAM is available for histone methylation (Papsdorf and Brunet, 2019). Consistent with this report, along with an increase in PC levels, regulation of histone H3-K36 methylation was observed in the liver, with GO down-regulated (Figs. 6c and 5b).

Phosphatidylethanolamine (PE) can modulate autophagy and protect against age-related diseases (Rockenfeller et al., 2015). PE supplementation increased both the mean and maximum lifespan in *C.elegans* (Park et al., 2021). When compared to NO, PE decreased with age in VO (Fig. 6d). Lysophosphatidylcholine (LPC) levels in human blood tend to decline with age, and low LPC levels have been linked to impaired mitochondrial oxidative capacity (Johnson and Stolzing, 2019). LPC levels that were lower in NO than in NY were higher in VO than in NO (Fig. 6d). LPI (20:4) levels in mice serum were found to decrease with age (Eum et al., 2020). Although LPI (20:4) levels in NO were lower than in NY, they were higher in VO (Fig. 6d).

These findings suggest that vutiglabridin may help alleviate lipid metabolism changes in elderly mice. Thus, vitiglabridin may have anti-ageing effects in mice by alleviating metabolic dysfunction.

4. Discussion

Many recent studies have been conducted to close the gap between lifespan and healthspan (Garmany et al., 2021; Campisi et al., 2019). With age, cellular function, including mitochondrial function, deteriorates (Amorim et al., 2022). Mitochondrial dysfunction can result in age-related metabolic dysfunctions (Amorim et al., 2022) and changes in ECM homeostasis. To address these metabolic dysfunctions, anti-ageing agents such as metformin, resveratrol, and rapamycin were developed and studied (Amorim et al., 2022). Because different factors contribute to ageing, different anti-ageing drugs must be developed to respond appropriately. Because vutiglabridin can act as an agonist in the electron transport chain (ETC) of mitochondria, improving mitochondrial function (Shin et al., 2021; Kang et al., 2022), we investigated whether it has anti-ageing properties. Administration of high doses of vutiglabridin unexpectedly caused weight loss in the aged mice, which resulted in death in the aged mice (not shown). Therefore, the experiment was conducted by selecting a dose that did not significantly affect the body weight of aged mice. In aged mice, a 50mpk dose of vutiglabridin alleviates ageing without causing changes in body weight. Vutiglabridin reduced SA-β-gal activity in the spleen, kidney, and liver of elderly mice. These findings supported our RT-qPCR findings that *Cdkn2a* expression decreased in aged mice, including GA muscle. We discovered that vutiglabridin had a significant effect on the spleen but had little effect on the kidney using RT-qPCR.

Using GO analysis, we discovered that in the GA muscle, ECM and mitochondria biogenesis were increased while ROS and RNA splicing were decreased. When compared to NO, many ECM signalling-related gene expressions, such as collagen, fibronectin, FGF, and integrin, were altered in the VO in a similar direction to NY. Furthermore, vutiglabridin had the ability to stabilize the expression of matrix remodelling enzyme-related genes as well as mitochondria morphology-related genes. Thus, vutiglabridin may improve muscle homeostasis in elderly mice by altering ECM niche and satellite cell function expression.

Insulin resistance, inflammation, and NAD^+ metabolism were found to be improved in aged eWAT, while mitochondrial ETC impairment and inflammation were found to be improved in the aged liver. Vutiglabridin treatment also increased the GSH/GSSG ratio. Vutiglabridin treatment alleviated the changes in lipid species such as ceramide, PC, PE, LPC, and LPI that increase with age. As a result, vutiglabridin is thought to slow ageing by improving metabolism. We hypothesised that these effects were caused by vutiglabridin's ability to improve mitochondrial functions, rescuing from metabolic dysfunctions. Because many metabolic enzymes can "moonlight" as RNA-binding proteins (RBPs), mitochondrial restoration affects metabolism and mRNA translation (Castello et al., 2015). Furthermore, ECM regulates metabolism (Ge et al., 2021), which may be reversible due to the close relationship between mitochondrial dysfunction and oxidative stress (Bhatti et al., 2017). A recent study found that mitochondrial translation is required for cytotoxic T-cell function by regulating the expression of cytotoxic proteins (Lisci et al., 2021). Reduced ROS stress can help to preserve mtDNA. Incompletely assembled matrix subunits produce superoxide

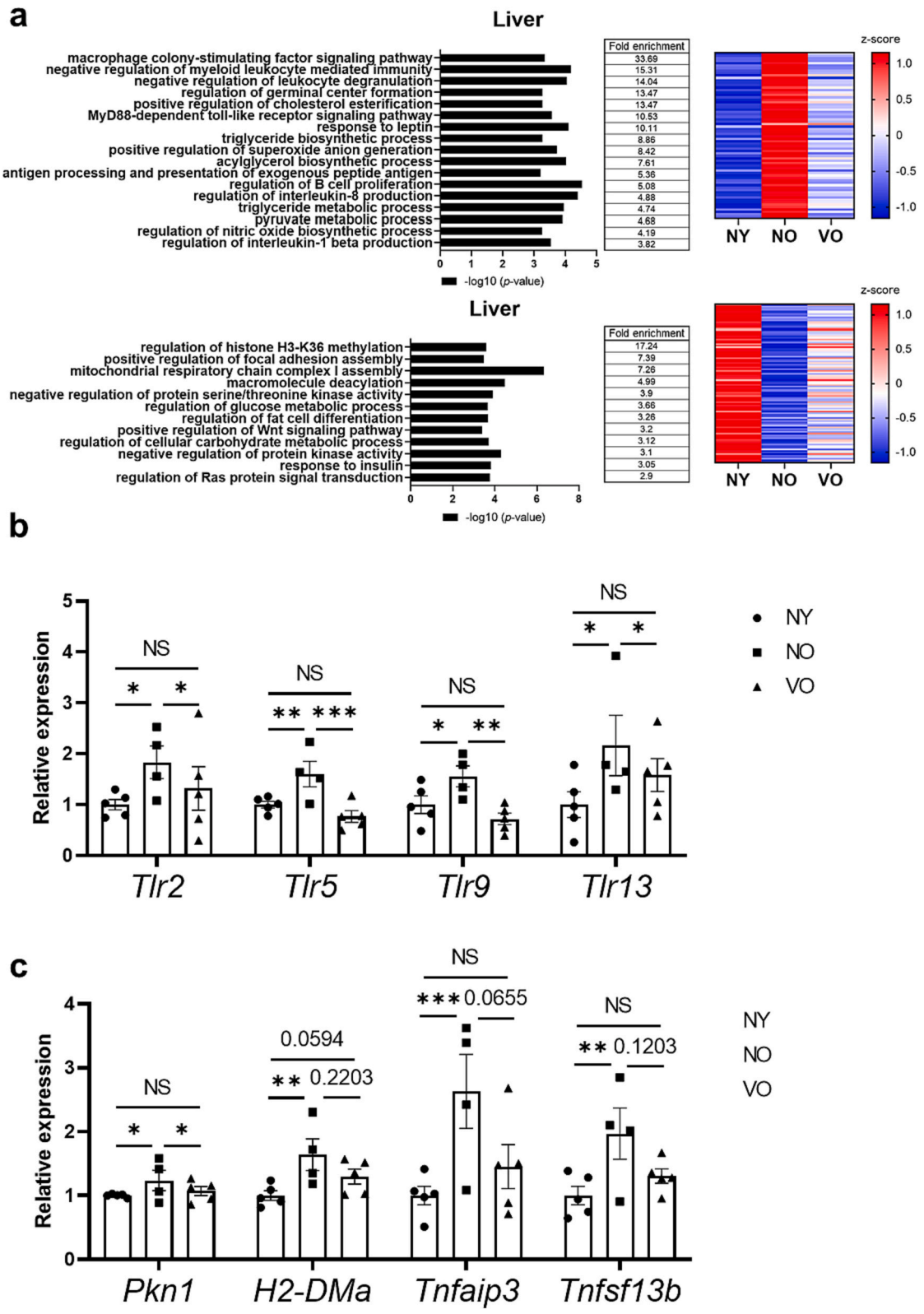

Fig. 5. Vutiglabridin reduces inflammageing and improves mitochondrial complex I assembly. (a) Top; Biological processes (BP) for genes that were up-regulated with ageing but were alleviated by vutiglabridin treatment in the liver (right). Heatmap represents the expression levels of genes belonging to the biological processes (left). Bottom; Biological processes (BP) for genes that were down-regulated with ageing but were alleviated by vutiglabridin treatment in the liver (right). Heatmap represents the expression levels of genes belonging to the biological processes (left). a, Expression was normalized by NY; (b) Relative expression of the toll-like receptor genes; (c) Relative expression of GC formation-associated genes; (d) Relative expression of lymphocyte homing and compartmentalization genes; (e) Relative expression of *Ccl2* and *Ccr2*; (f) Relative expression of M1 macrophage marker, *Cd80*; (g) Relative expression of M2 macrophage marker, *Mrc1*; (h) Relative GSH/GSSG ratio; (i) Relative gene expression of mitochondrial complex I membrane subunit, *Ndufa5,* and *Ndufb2*. n of NY, NO, and VO was 5, 4, and 5, respectively. Data are mean ± s.e.m., NS, not significant; $^{*}P < 0.05$, $^{**}P < 0.01$, $^{***}P < 0.001$. Unpaired two-tailed *t*-test.

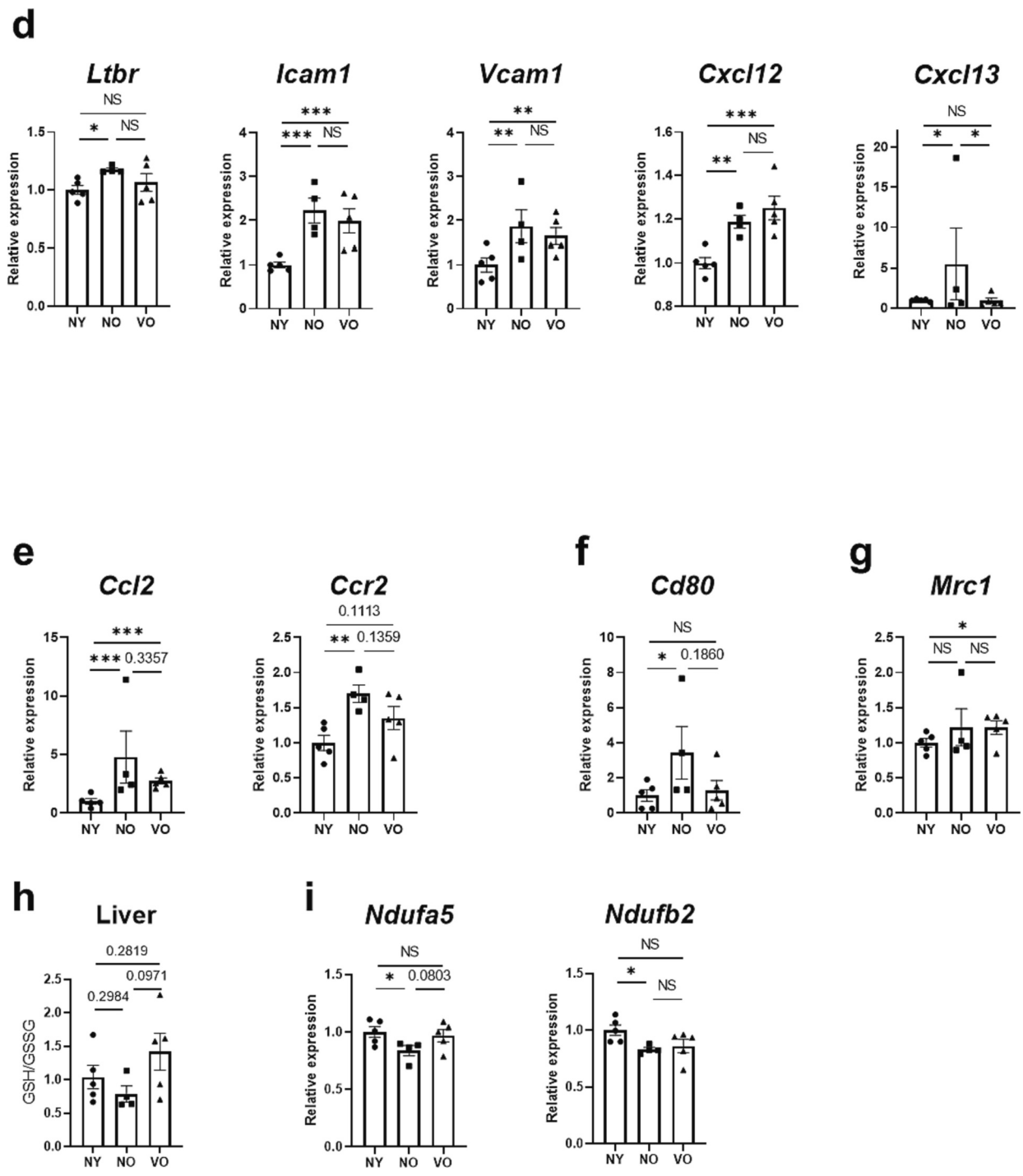

Fig. 5. (*continued*).

and reduce ATP production when mitochondrial complex I membrane subunits are not expressed (Miwa et al., 2014). Reduced mtDNA damage would thus restore ETCs' ability to produce ATP and NAD^+ as needed, while also lowering ROS production. In addition, some studies have linked mitochondrial dysfunction to insulin resistance (Petersen et al., 2003; Kim et al., 2008). Reduced insulin resistance in VO was thus attributed to improved mitochondrial function.

Vutiglabridin reduces inflammation, according to the results of the liver and eWAT tests. In the liver and eWAT, vutiglabridin treatment reduced TLO formation, which indicates chronic inflammation, as well as pro-inflammatory T cells and M1 macrophages. According to a recent study, metformin reduces inflammation by normalizing mitochondrial function (Bharath et al., 2020). Investigating whether vutiglabridin reduces inflammation would thus be an appropriate research topic.

The following additional studies are needed to confirm the above-mentioned findings. Muscle regeneration and function should be confirmed after inducing the bilateral cardiotoxin (CTX) injury in the GA muscle of aged mice to confirm the effects related to muscle homeostasis (Sahu et al., 2021). Extracellular acidification rate (ECAR) and oxygen consumption rate (OCR), which indicate glycolysis and OXPHOS, respectively, could be used to confirm mitochondrial function. A glucose tolerance and insulin tolerance test would be performed to see if vutiglabridin treatment improved insulin sensitivity. Western blot analysis and other signalling-associated proteins should be used to confirm

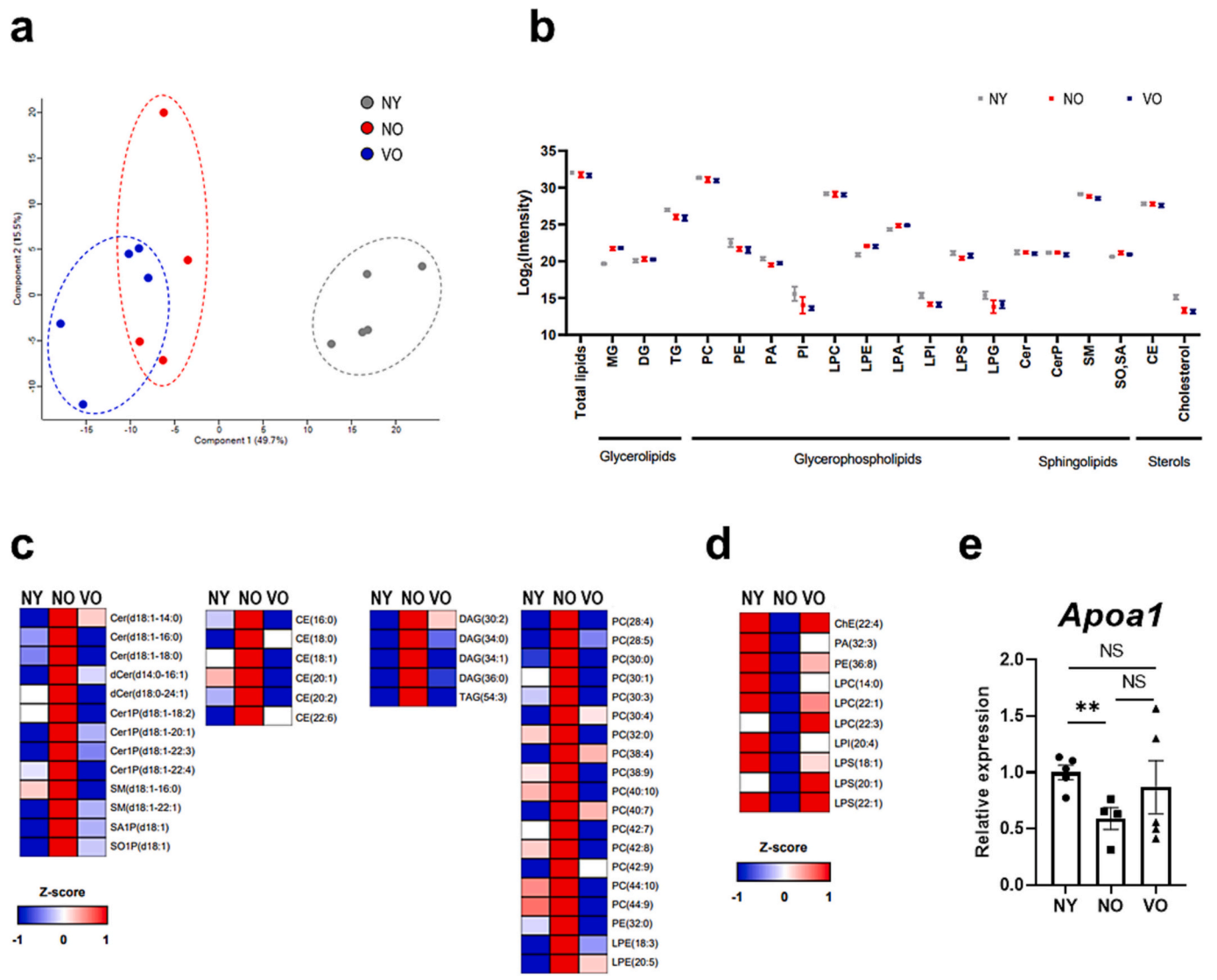

Fig. 6. Vutiglabridin alleviates ageing-related lipid profile changes. (a) Principal coordinate analysis of serum total lipids levels in the NY, NO, and VO; (b) Overall lipid composition in the NY, NO, and VO; (c) Lipid species increased with ageing and decreased by vutiglabridin treatment; (d) Lipid species decreased with ageing and increased by vutiglabridin treatment. The expression of each lipid species was expressed as a z-score; (e) Relative *Apoa1* expression in the liver. n of NY, NO, and VO was 5, 4, and 5, respectively. Data are mean ± s.e.m., NS, not significant; $^{*}P < 0.05$, $^{**}P < 0.01$, $^{***}P < 0.001$.

whether increased mRNA levels of MAPK8 phosphorylated the IRS protein in NO. The number of individuals in each group should be increased to reduce variance and to see a clear difference between NO and VO.

Vutiglabridin improves mitochondrial function and thereby reduces intracellular oxidative stress (Kang et al., 2022; Choi et al., 2021; Heo et al., 2023). Vutiglabridin also activates autophagic flux to autolysosomes (Shin et al., 2021). It has been reported that the AMPK signalling pathway controls the ageing process such as metabolic regulation, increasing oxidative stress and reducing autophagic clearance (Salminen and Kaarniranta, 2012). Further studies on the AMPK pathway as an anti-ageing effect of vutiglabridin will reveal the anti-ageing mechanism of vutiglabridin more clearly.

Fundings

This work was supported by the DGIST R&D Program of the Ministry of Science and ICT (22-BRP-01 for Jooseung Hyeon, Jihan Lee and Chang-Hoon Nam) and by the GRRC program of Gyeonggi province [(GRRC Kyung Hee 2023-B01), Industrial Application Research of Medicinal, Pharmaceutical and Chemical Materials] for Eunju Kim and Kwang Pyo Kim.

Ethics approval

The study was approved by the Ethical Committee of Animal Research of Daegu Gyeongbuk Institute of Science and Technology, Daegu, South Korea (DGIST-IACUC-21070701-00).

CRediT authorship contribution statement

Jooseung Hyeon: Conceptualization, Validation, Methodology, Formal analysis, Investigation, Writing – original draft. **Jihan Lee:** Conceptualization, Validation, Methodology, Formal analysis, Investigation, Writing – original draft. **Eunju Kim:** Methodology, Validation, Investigation, Data curation. **Hyeong Min Lee:** Methodology, Validation, Investigation, Data curation. **Kwang Pyo Kim:** Resources, Supervision, Funding acquisition, Writing – review & editing. **Jaejin Shin:**

Conceptualization, Validation, Writing – review & editing. **Hyung Soon Park:** Resources, Supervision. **Yun-Il Lee:** Validation, Writing – review & editing. **Chang-Hoon Nam:** Conceptualization, Validation, Resources, Supervision, Funding acquisition, Writing – review & editing.

Declaration of competing interest

Hyeong Min Lee, Jaejin Shin and Hyung Soon Park are current employees of Glaceum Inc. and hold its stocks/shares. Glaceum Inc. owns the intellectual property rights of vutiglabridin. The remaining authors declare no competing interests.

Data availability

Data will be made available on request to corresponding author. Chang-Hoon Nam (chang@dgist.ac.kr). Ageing and Immunity Laboratory, Department of New Biology, Daegu Gyeongbuk Institute of Science and Technology, Daegu, 42988, Republic of Korea.

Acknowledgments

We would like to thank everyone who participated in or assisted with this research, as well as Daegu Gyeongbuk Institute of Science and Technology for their financial assistance.

Appendix A. Supplementary data

Supplementary data to this article can be found online at https://doi.org/10.1016/j.exger.2023.112269.

References

Alcazar, O., Cousins, S.W., Marin-Castaño, M.E., 2007. MMP-14 and TIMP-2 overexpression protects against hydroquinone-induced oxidant injury in RPE: implications for extracellular matrix turnover. Invest. Ophthalmol. Vis. Sci. 48 (12), 5662–5670 (Dec).

Aloisi, F., Pujol-Borrell, R., 2006. Lymphoid neogenesis in chronic inflammatory diseases. Nat. Rev. Immunol. 6 (3), 205–217 (Mar).

Amen, O.M., Sarker, S.D., Ghildyal, R., Arya, A., 2019. Endoplasmic reticulum stress activates unfolded protein response signaling and mediates inflammation, obesity, and cardiac dysfunction: therapeutic and molecular approach. Front. Pharmacol. 10 (10), 977 (Sep).

Amorim, J.A., Coppotelli, G., Rolo, A.P., Palmeira, C.M., Ross, J.M., Sinclair, D.A., 2022. Mitochondrial and metabolic dysfunction in ageing and age-related diseases. Nat. Rev. Endocrinol. 18 (4), 243–258 (Apr).

An, J.N., Kim, H., Kim, E.N., Cho, A., Cho, Y., Choi, Y.W., Kim, J.H., Yang, S.H., Choi, B. S., Lim, C.S., Kim, Y.S., Kim, K.P., Lee, J.P., 2021. Effects of periostin deficiency on kidney aging and lipid metabolism. Aging (Albany NY) 13 (19), 22649–22665 (Oct 3).

Aunan, J.R., Watson, M.M., Hagland, H.R., Søreide, K., 2016. Molecular and biological hallmarks of ageing. Br. J. Surg. 103 (2), e29–e46 (Jan).

Bejarano, E., Murray, J.W., Wang, X., Pampliega, O., Yin, D., Patel, B., Yuste, A., Wolkoff, A.W., Cuervo, A.M., 2018. Defective recruitment of motor proteins to autophagic compartments contributes to autophagic failure in aging. Aging Cell 17 (4) (Aug). (e12777).

Benayoun, B.A., Pollina, E.A., Singh, P.P., Mahmoudi, S., Harel, I., Casey, K.M., Dulken, B.W., Kundaje, A., Brunet, A., 2019. Remodeling of epigenome and transcriptome landscapes with aging in mice reveals widespread induction of inflammatory responses. Genome Res. 29 (4), 697–709 (Apr).

Bénézech, C., Luu, N.T., Walker, J.A., Kruglov, A.A., Loo, Y., Nakamura, K., Zhang, Y., Nayar, S., Jones, L.H., Flores-Langarica, A., McIntosh, A., Marshall, J., Barone, F., Besra, G., Miles, K., Allen, J.E., Gray, M., Kollias, G., Cunningham, A.F., Withers, D. R., Toellner, K.M., Jones, N.D., Veldhoen, M., Nedospasov, S.A., McKenzie, A.N.J., Caamaño, J.H., 2015. Inflammation-induced formation of fat-associated lymphoid clusters. Nat. Immunol. 16 (8), 819–828 (Aug).

Bharath, L.P., Agrawal, M., McCambridge, G., Nicholas, D.A., Hasturk, H., Liu, J., Jiang, K., Liu, R., Guo, Z., Deeney, J., Apovian, C.M., Snyder-Cappione, J., Hawk, G. S., Fleeman, R.M., Pihl, R.M.F., Thompson, K., Belkina, A.C., Cui, L., Proctor, E.A., Kern, P.A., Nikolajczyk, B.S., 2020. Metformin enhances autophagy and normalizes mitochondrial function to alleviate aging-associated inflammation. Cell Metab. 32 (1), 44–55.e6 (Jul 7).

Bhatti, J.S., Bhatti, G.K., Reddy, P.H., 2017. Mitochondrial dysfunction and oxidative stress in metabolic disorders a step towards mitochondria based therapeutic strategies. Biochim. Biophys. Acta Mol. basis Dis. 1863 (5), 1066–1077 (May).

Breil, C., Abert Vian, M., Zemb, T., Kunz, W., Chemat, F., 2017. "Bligh and dyer" and Folch methods for solid–liquid–liquid extraction of lipids from microorganisms. Comprehension of solvatation mechanisms and towards substitution with alternative solvents. Int. J. Mol. Sci. 18 (4), 708 (Mar 27).

Buckingham, M., Rigby, P.W., 2014. Gene regulatory networks and transcriptional mechanisms that control myogenesis. Dev. Cell 28 (3), 225–238 (Feb 10).

Camell, C.D., Sander, J., Spadaro, O., Lee, A., Nguyen, K.Y., Wing, A., Goldberg, E.L., Youm, Y.H., Brown, C.W., Elsworth, J., Rodeheffer, M.S., Schultze, J.L., Dixit, V.D., 2017. Inflammasome-driven catecholamine catabolism in macrophages blunts lipolysis during ageing. Nature 550 (7674), 119–123 (Oct 5).

Camell, C.D., Günther, P., Lee, A., Goldberg, E.L., Spadaro, O., Youm, Y.H., Bartke, A., Hubbard, G.B., Ikeno, Y., Ruddle, N.H., Schultze, J., Dixit, V.D., 2019. Aging induces an Nlrp3 inflammasome-dependent expansion of adipose B cells that impairs metabolic homeostasis. Cell Metab. 30 (6), 1024–1039 (Dec 3, e6).

Campisi, J., Kapahi, P., Lithgow, G.J., Melov, S., Newman, J.C., Verdin, E., 2019. From discoveries in ageing research to therapeutics for healthy ageing. Nature 571 (7764), 183–192 (Jul).

Castello, A., Hentze, M.W., Preiss, T., 2015. Metabolic enzymes enjoying new partnerships as RNA-binding proteins. Trends Endocrinol. Metab. 26 (12), 746–757 (Dec).

Chawla, A., Nguyen, K.D., Goh, Y.P., 2011. Macrophage-mediated inflammation in metabolic disease. Nat. Rev. Immunol. 11 (11), 738–749 (Oct 10).

Chen, Keng, Wang, Yilin, Deng, Xiaoying, Guo, Ling, Chuanyue, Wu., 2021. Extracellular matrix stiffness regulates mitochondrial dynamics through PINCH-1- and kindlin-2-mediated signalling. Curr. Res. Cell Biol. 2 (100008), 2590–2636.

Chini, C.C.S., Peclat, T.R., Warner, G.M., Kashyap, S., Espindola-Netto, J.M., de Oliveira, G.C., Gomez, L.S., Hogan, K.A., Tarragó, M.G., Puranik, A.S., Agorrody, G., Thompson, K.L., Dang, K., Clarke, S., Childs, B.G., Kanamori, K.S., Witte, M.A., Vidal, P., Kirkland, A.L., De Cecco, M., Chellappa, K., McReynolds, M.R., Jankowski, C., Tchkonia, T., Kirkland, J.L., Sedivy, J.M., van Deursen, J.M., Baker, D.J., van Schooten, W., Rabinowitz, J.D., Baur, J.A., Chini, E.N., 2020. CD38 ecto-enzyme in immune cells is induced during aging and regulates NAD+ and NMN levels. Nat. Metab. 2 (11), 1284–1304 (Nov).

Choi, L.S., Jo, I.G., Kang, K.S., Im, J.H., Kim, J., Kim, J., Chung, J.W., Yoo, S.K., 2021. Discovery and preclinical efficacy of HSG4112, a synthetic structural analog of glabridin, for the treatment of obesity. Int. J. Obes. 45 (1), 130–142 (Jan).

Covarrubias, A., Byles, V., Horng, T., 2013. ROS sets the stage for macrophage differentiation. Cell Res. 23 (8), 984–985 (Aug).

Covarrubias, A.J., Kale, A., Perrone, R., Lopez-Dominguez, J.A., Pisco, A.O., Kasler, H.G., Schmidt, M.S., Heckenbach, I., Kwok, R., Wiley, C.D., Wong, H.S., Gibbs, E., Iyer, S. S., Basisty, N., Wu, Q., Kim, I.J., Silva, E., Vitangcol, K., Shin, K.O., Lee, Y.M., Riley, R., Ben-Sahra, I., Ott, M., Schilling, B., Scheibye-Knudsen, M., Ishihara, K., Quake, S.R., Newman, J., Brenner, C., Campisi, J., Verdin, E., 2020. Senescent cells promote tissue NAD+ decline during ageing via the activation of CD38+ macrophages. Nat. Metab. 2 (11), 1265–1283 (Nov).

Covarrubias, A.J., Perrone, R., Grozio, A., Verdin, E., 2021. NAD+ metabolism and its roles in cellular processes during ageing. Nat. Rev. Mol. Cell Biol. 22 (2), 119–141 (Feb).

Crimmins, E.M., 2015. Lifespan and healthspan: past, present, and promise. Gerontologist 55 (6), 901–911 (Dec).

Csapo, R., Gumpenberger, M., Wessner, B., 2020. Skeletal muscle extracellular matrix - what do we know about its composition, regulation, and physiological roles? A narrative review. Front. Physiol. 19 (11), 253 (Mar).

Eum, J.Y., Lee, J.C., Yi, S.S., Kim, I.Y., Seong, J.K., Moon, M.H., 2020. Aging-related lipidomic changes in mouse serum, kidney, and heart by nanoflow ultrahigh-performance liquid chromatography-tandem mass spectrometry. J. Chromatogr. A 10 (1618), 460849 (May).

Feng, Z., Hanson, R.W., Berger, N.A., Trubitsyn, A., 2016. Reprogramming of energy metabolism as a driver of aging. Oncotarget 7 (13), 15410–15420 (Mar 29).

Franceschi, C., Garagnani, P., Morsiani, C., Conte, M., Santoro, A., Grignolio, A., Monti, D., Capri, M., Salvioli, S., 2018. The continuum of aging and age-related diseases: common mechanisms but different rates. Front. Med. (Lausanne) 12 (5), 61 (Mar).

Frontini, M.J., Nong, Z., Gros, R., Drangova, M., O'Neil, C., Rahman, M.N., Akawi, O., Yin, H., Ellis, C.G., Pickering, J.G., 2011. Fibroblast growth factor 9 delivery during angiogenesis produces durable, vasoresponsive microvessels wrapped by smooth muscle cells. Nat. Biotechnol. 29 (5), 421–427 (May).

Garmany, A., Yamada, S., Terzic, A., 2021. Longevity leap: mind the healthspan gap. NPJ Regen. Med. 6 (1), 57 (Sep 23).

Gattazzo, F., Urciuolo, A., Bonaldo, P., 2014. Extracellular matrix: a dynamic microenvironment for stem cell niche. Biochim. Biophys. Acta 1840 (8), 2506–2519 (Aug).

Ge, H., Tian, M., Pei, Q., Tan, F., Pei, H., 2021. Extracellular matrix stiffness: new areas affecting cell metabolism. Front. Oncol. 24 (11), 631991 (Feb).

Gomes, L.R., Terra, L.F., Wailemann, R.A., Labriola, L., Sogayar, M.C., 2012. TGF-β1 modulates the homeostasis between MMPs and MMP inhibitors through p38 MAPK and ERK1/2 in highly invasive breast cancer cells. BMC Cancer 19 (12), 26 (Jan).

Gomes, A.P., Price, N.L., Ling, A.J., Moslehi, J.J., Montgomery, M.K., Rajman, L., White, J.P., Teodoro, J.S., Wrann, C.D., Hubbard, B.P., Mercken, E.M., Palmeira, C. M., de Cabo, R., Rolo, A.P., Turner, N., Bell, E.L., Sinclair, D.A., 2013. Declining NAD (+) induces a pseudohypoxic state disrupting nuclear-mitochondrial communication during aging. Cell 155 (7), 1624–1638 (Dec 19).

Gong, T., Liu, L., Jiang, W., Zhou, R., 2020. DAMP-sensing receptors in sterile inflammation and inflammatory diseases. Nat. Rev. Immunol. 20 (2), 95–112 (Feb).

He, M., Chiang, H.H., Luo, H., Zheng, Z., Qiao, Q., Wang, L., Tan, M., Ohkubo, R., Mu, W. C., Zhao, S., Wu, H., Chen, D., 2020. An acetylation switch of the NLRP3 inflammasome regulates aging-associated chronic inflammation and insulin resistance. Cell Metab. 31 (3), 580–591 (Mar 3, e5).

Heino, J., 2014. Cellular signaling by collagen-binding integrins. Adv. Exp. Med. Biol. 819, 143–155.
Heo, J.W., Lee, H.E., Lee, J., Choi, L.S., Shin, J., Mun, J.Y., Park, H.S., Park, S.C., Nam, C. H., 2023 Feb. Vutiglabridin alleviates cellular senescence process of dysfunctional replication, metabolic regulation, and circadian clock in primary human dermal fibroblasts. bioRxiv. https://doi.org/10.1101/2023.02.12.528227.
Heymann, F., Tacke, F., 2016. Immunology in the liver—from homeostasis to disease. Nat. Rev. Gastroenterol. Hepatol. 13 (2), 88–110 (Feb).
Huang, X., Withers, B.R., Dickson, R.C., 2014. Sphingolipids and lifespan regulation. Biochim. Biophys. Acta 1841 (5), 657–664 (May).
Jablonski, K.A., Amici, S.A., Webb, L.M., Ruiz-Rosado Jde, D., Popovich, P.G., Partida-Sanchez, S., Guerau-de-Arellano, M., 2015. Novel markers to delineate murine M1 and M2 macrophages. PLoS One 10 (12), e0145342 (Dec 23).
Jannone, G., Rozzi, M., Najimi, M., Decottignies, A., Sokal, E.M., 2020. An optimized protocol for histochemical detection of senescence-associated Beta-galactosidase activity in cryopreserved liver tissue. J. Histochem. Cytochem. 68 (4), 269–278 (Apr).
Johnson, A.A., Stolzing, A., 2019. The role of lipid metabolism in aging, lifespan regulation, and age-related disease. Aging Cell 18 (6), e13048 (Dec).
Kalathookunnel Antony, A., Lian, Z., Wu, H., 2018. T cells in adipose tissue in aging. Front. Immunol. (9), 2945 (Dec 12).
Kang, S., Choi, L.S., Im, S., Kim, J.H., Lee, K.W., Kim, D.H., Park, J.H., Park, M.H., Lee, J., Park, S.K., Kim, K.P., Lee, H.M., Jeon, H.J., Park, H.S., Yoo, S.K., Kim, Pak Y., 2022. Vutiglabridin Improves Neurodegeneration in MPTP-Induced Parkinson's Disease Mice by Targeting Mitochondrial Paraoxonase-2. bioRxiv. https://doi.org/10.1101/2022.10.20.512990 (Oct).
Kaushik, S., Cuervo, A.M., 2015. Proteostasis and aging. Nat. Med. 21 (12), 1406–1415 (Dec).
Kim, J.A., Wei, Y., Sowers, J.R., 2008. Role of mitochondrial dysfunction in insulin resistance. Circ. Res. 102 (4), 401–414 (Feb 29).
Kimura, S., Noda, T., Yoshimori, T., 2008. Dynein-dependent movement of autophagosomes mediates efficient encounters with lysosomes. Cell Struct. Funct. 33 (1), 109–122.
Lee, J.W., Nishiumi, S., Yoshida, M., Fukusaki, E., Bamba, T., 2013. Simultaneous profiling of polar lipids by supercritical fluid chromatography/tandem mass spectrometry with methylation. J. Chromatogr. A 1 (1279), 98–107 (Mar).
Lee, J.W., Shinohara, H., Jung, J.H., Mok, H.J., Akao, Y., Kim, K.P., 2016. Detailed characterization of alterations in the lipid profiles during autophagic cell death of leukemia cells. RSC Adv. 6 (35), 29512–29518.
Leitinger, B., 2014. Discoidin domain receptor functions in physiological and pathological conditions. Int. Rev. Cell Mol. Biol. 310, 39–87.
Lisci, M., Barton, P.R., Randzavola, L.O., Ma, C.Y., Marchingo, J.M., Cantrell, D.A., Paupe, V., Prudent, J., Stinchcombe, J.C., Griffiths, G.M., 2021. Mitochondrial translation is required for sustained killing by cytotoxic T cells. Science 374 (6565), eabe9977 (Oct 15).
Liu, L., Su, X., Quinn 3rd, W.J., Hui, S., Krukenberg, K., Frederick, D.W., Redpath, P., Zhan, L., Chellappa, K., White, E., Migaud, M., Mitchison, T.J., Baur, J.A., Rabinowitz, J.D., 2018. Quantitative analysis of NAD synthesis-breakdown fluxes. Cell Metab. 27 (5), 1067–1080 (May 1, e5).
Liu, L., Guo, H., Song, A., Huang, J., Zhang, Y., Jin, S., Li, S., Zhang, L., Yang, C., Yang, P., 2020. Progranulin inhibits LPS-induced macrophage M1 polarization via NF-κB and MAPK pathways. BMC Immunol. 21 (1), 32 (Jun 5).
Liu, X., Wang, K., Hou, S., Jiang, Q., Ma, C., Zhao, Q., Kong, L., Chen, J., Wang, Z., Zhang, H., Yuan, T., Li, Y., Huan, Y., Shen, Z., Hu, Z., Huang, Z., Cui, B., Li, P., 2022. Insulin induces insulin receptor degradation in the liver through EphB4. Nat. Metab. 4 (9), 1202–1213 (Sep).
López-Armada, M.J., Riveiro-Naveira, R.R., Vaamonde-García, C., Valcárcel-Ares, M.N., 2013. Mitochondrial dysfunction and the inflammatory response. Mitochondrion 13 (2), 106–118 (Mar).
López-Otín, C., Blasco, M.A., Partridge, L., Serrano, M., Kroemer, G., 2013. The hallmarks of aging. Cell 153 (6), 1194–1217 (Jun 6).
Love, Michael, Anders, Simon, Huber, Wolfgang, 2014. Beginner's guide to using the DESeq2 package. Genome Biol. 15, 550.
Lumeng, C.N., Liu, J., Geletka, L., Delaney, C., Delproposto, J., Desai, A., Oatmen, K., Martinez-Santibanez, G., Julius, A., Garg, S., Yung, R.L., 2011. Aging is associated with an increase in T cells and inflammatory macrophages in visceral adipose tissue. J. Immunol. 187 (12), 6208–6216 (Dec 15).
Lutz, W., Sanderson, W., Scherbov, S., 2008. The coming acceleration of global population ageing. Nature 451 (7179), 716–719 (Feb 7).
Martinon, F., Mayor, A., Tschopp, J., 2009. The inflammasomes: guardians of the body. Annu. Rev. Immunol. 27, 229–265.
Martins, S.G., Zilhão, R., Thorsteinsdóttir, S., Carlos, A.R., 2021. Linking oxidative stress and DNA damage to changes in the expression of extracellular matrix components. Front. Genet. 29 (12), 673002 (Jul).
McNelis, J.C., Olefsky, J.M., 2014. Macrophages, immunity, and metabolic disease. Immunity 41 (1), 36–48 (Jul 17).
Melouane, A., Yoshioka, M., St-Amand, J., 2020. Extracellular matrix/mitochondria pathway: a novel potential target for sarcopenia. Mitochondrion 50, 63–70 (Jan).
Melzer, D., Pilling, L.C., Ferrucci, L., 2020. The genetics of human ageing. Nat. Rev. Genet. 21 (2), 88–101 (Feb).
Miwa, S., Jow, H., Baty, K., Johnson, A., Czapiewski, R., Saretzki, G., Treumann, A., von Zglinicki, T., 2014. Low abundance of the matrix arm of complex I in mitochondria predicts longevity in mice. Nat. Commun. 12 (5), 3837 (May).
Montoliu, I., Scherer, M., Beguelin, F., DaSilva, L., Mari, D., Salvioli, S., Martin, F.P., Capri, M., Bucci, L., Ostan, R., Garagnani, P., Monti, D., Biagi, E., Brigidi, P., Kussmann, M., Rezzi, S., Franceschi, C., Collino, S., 2014. Serum profiling of healthy aging identifies phospho- and sphingolipid species as markers of human longevity. Aging (Albany NY) 6 (1), 9–25 (Jan).
Moon, S.K., Cha, B.Y., Lee, Y.C., Nam, K.S., Runge, M.S., Patterson, C., Kim, C.H., 2004. Age-related changes in matrix metalloproteinase-9 regulation in cultured mouse aortic smooth muscle cells. Exp. Gerontol. 39 (1), 123–131 (Jan).
Muñoz-Cánoves, P., Neves, J., Sousa-Victor, P., 2020. Understanding muscle regenerative decline with aging: new approaches to bring back youthfulness to aged stem cells. FEBS J. 287 (3), 406–416 (Feb).
Mutlu, A.S., Duffy, J., Wang, M.C., 2021. Lipid metabolism and lipid signals in aging and longevity. Dev. Cell 56 (10), 1394–1407 (May 17).
Navarro, A., Boveris, A., 2004. Rat brain and liver mitochondria develop oxidative stress and lose enzymatic activities on aging. Am. J. Phys. Regul. Integr. Comp. Phys. 287 (5). Nov. (R1244–9).
Ori, A., Toyama, B.H., Harris, M.S., Bock, T., Iskar, M., Bork, P., Ingolia, N.T., Hetzer, M. W., Beck, M., 2015. Integrated transcriptome and proteome analyses reveal organ-specific proteome deterioration in old rats. Cell Syst. 1 (3), 224–237 (Sep 23).
Pallafacchina, G., François, S., Regnault, B., Czarny, B., Dive, V., Cumano, A., Montarras, D., Buckingham, M., 2010. An adult tissue-specific stem cell in its niche: a gene profiling analysis of in vivo quiescent and activated muscle satellite cells. Stem Cell Res. 4 (2), 77–91 (Mar).
Papsdorf, K., Brunet, A., 2019. Linking lipid metabolism to chromatin regulation in aging. Trends Cell Biol. 29 (2), 97–116 (Feb).
Paradis, S., Charles, A.L., Georg, I., Goupilleau, F., Meyer, A., Kindo, M., Laverny, G., Metzger, D., Geny, B., 2019. Aging exacerbates ischemia-reperfusion-induced mitochondrial respiration impairment in skeletal muscle. Antioxidants (Basel). 8 (6), 168 (Jun 8).
Park, S., Kim, B.K., Park, S.K., 2021. Supplementation with phosphatidylethanolamine confers anti-oxidant and anti-aging effects via hormesis and reduced insulin/IGF-1-like signaling in C. elegans. Mech. Ageing Dev. 197, 111498 (Jul).
Partridge, L., Deelen, J., Slagboom, P.E., 2018. Facing up to the global challenges of ageing. Nature 561 (7721), 45–56 (Sep).
Pawlikowski, B., Vogler TO, Gadek, K., Olwin, B.B., 2017. Regulation of skeletal muscle stem cells by fibroblast growth factors. Dev. Dyn. 246 (5), 359–367 (May).
Pérez, V.I., Buffenstein, R., Masamsetti, V., Leonard, S., Salmon, A.B., Mele, J., Andziak, B., Yang, T., Edrey, Y., Friguet, B., Ward, W., Richardson, A., Chaudhuri, A., 2009. Protein stability and resistance to oxidative stress are determinants of longevity in the longest-living rodent, the naked mole-rat. Proc. Natl. Acad. Sci. U. S. A. 106 (9), 3059–3064 (Mar 3).
Petersen, K.F., Befroy, D., Dufour, S., Dziura, J., Ariyan, C., Rothman, D.L., DiPietro, L., Cline, G.W., Shulman, G.I., 2003. Mitochondrial dysfunction in the elderly: possible role in insulin resistance. Science 300 (5622), 1140–1142 (May 16).
Place, D.E., Kanneganti, T.D., 2018. Recent advances in inflammasome biology. Curr. Opin. Immunol. 50, 32–38 (Feb).
Podhorecka, M., Ibanez, B., Dmoszyńska, A., 2017. Metformin – its potential anti-cancer and anti-aging effects. Postepy Hig. Med. Dosw. (Online) 71 (0), 170–175 (Mar 2).
Pontzer, H., Yamada, Y., Sagayama, H., Ainslie, P.N., Andersen, L.F., Anderson, L.J., Arab, L., Baddou, I., Bedu-Addo, K., Blaak, E.E., Blanc, S., Bonomi, A.G., Bouten, C.V. C., Bovet, P., Buchowski, M.S., Butte, N.F., Camps, S.G., Close, G.L., Cooper, J.A., Cooper, R., Das, S.K., Dugas, L.R., Ekelund, U., Entringer, S., Forrester, T., Fudge, B. W., Goris, A.H., Gurven, M., Hambly, C., El Hamdouchi, A., Hoos, M.B., Hu, S., Joonas, N., Joosen, A.M., Katzmarzyk, P., Kempen, K.P., Kimura, M., Kraus, W.E., Kushner, R.F., Lambert, E.V., Leonard, W.R., Lessan, N., Martin, C., Medin, A.C., Meijer, E.P., Morehen, J.C., Morton, J.P., Neuhouser, M.L., Nicklas, T.A., Ojiambo, R. M., Pietiläinen, K.H., Pitsiladis, Y.P., Plange-Rhule, J., Plasqui, G., Prentice, R.L., Rabinovich, R.A., Racette, S.B., Raichlen, D.A., Ravussin, E., Reynolds, R.M., Roberts, S.B., Schuit, A.J., Sjödin, A.M., Stice, E., Urlacher, S.S., Valenti, G., Van Etten, L.M., Van Mil, E.A., Wells, J.C.K., Wilson, G., Wood, B.M., Yanovski, J., Yoshida, T., Zhang, X., Murphy-Alford, A.J., Loechl, C., Luke, A.H., Rood, J., Schoeller, D.A., Westerterp, K.R., Wong, W.W., Speakman, J.R., 2021. IAEA DLW database consortium. Daily energy expenditure through the human life course. Science 373 (6556), 808–812 (Aug 13).
Rockenfeller, P., Koska, M., Pietrocola, F., Minois, N., Knittelfelder, O., Sica, V., Franz, J., Carmona-Gutierrez, D., Kroemer, G., Madeo, F., 2015. Phosphatidylethanolamine positively regulates autophagy and longevity. Cell Death Differ. 22 (3), 499–508 (Mar).
Royce, G.H., Brown-Borg, H.M., Deepa, S.S., 2019. The potential role of necroptosis in inflammaging and aging. Geroscience 41 (6), 795–811 (Dec).
Rubinsztein, D.C., Mariño, G., Kroemer, G., 2011. Autophagy and aging. Cell 146 (5), 682–695 (Sep 2).
Sahu, A., Clemens, Z.J., Shinde, S.N., Sivakumar, S., Pius, A., Bhatia, A., Picciolini, S., Carlomagno, C., Gualerzi, A., Bedoni, M., Van Houten, B., Lovalekar, M., Fitz, N.F., Lefterov, I., Barchowsky, A., Koldamova, R., Ambrosio, F., 2021. Regulation of aged skeletal muscle regeneration by circulating extracellular vesicles. Nat. Aging 1 (12), 1148–1161 (Dec).
Salminen, A., Kaarniranta, K., 2012. AMP-activated protein kinase (AMPK) controls the aging process via an integrated signaling network. Ageing Res. Rev. 11 (2), 230–241 (Apr).
Salminen, A., Kauppinen, A., Kaarniranta, K., 2012. Emerging role of NF-κB signaling in the induction of senescence-associated secretory phenotype (SASP). Cell. Signal. 24 (4), 835–845 (Apr).
Shin, G.C., Lee, H.M., Kim, N.Y., Yoo, S.K., Park, Y.S., Park, H.S., Ryo, D., Kim, K.P., Kim, K.H., 2021. Synthetic Glabridin Derivatives Mitigate Steatohepatitis in a Diet-induced Biopsy-confirmed Non-alcoholic Steatosis Hepatitis Mouse Model Through Paraoxonase-2. bioRxiv. https://doi.org/10.1101/2021.10.01.462722 (Oct).
Stegeman, R., Weake, V.M., 2017. Transcriptional signatures of aging. J. Mol. Biol. 429 (16), 2427–2437 (Aug 4).

Stein, G.H., Drullinger, L.F., Soulard, A., Dulić, V., 1999. Differential roles for cyclin-dependent kinase inhibitors p21 and p16 in the mechanisms of senescence and differentiation in human fibroblasts. Mol. Cell. Biol. 19 (3), 2109–2117 (Mar).
Stromsdorfer, K.L., Yamaguchi, S., Yoon, M.J., Moseley, A.C., Franczyk, M.P., Kelly, S.C., Qi, N., Imai, S., Yoshino, J., 2016. NAMPT-mediated NAD(+) biosynthesis in adipocytes regulates adipose tissue function and multi-organ insulin sensitivity in mice. Cell Rep. 16 (7), 1851–1860 (Aug 16).
Strowig, T., Henao-Mejia, J., Elinav, E., Flavell, R., 2012. Inflammasomes in health and disease. Nature 481 (7381), 278–286 (Jan 18).
Tyedmers, J., Mogk, A., Bukau, B., 2010. Cellular strategies for controlling protein aggregation. Nat. Rev. Mol. Cell Biol. 11 (11), 777–788. Nov.
Westermann, B., 2010. Mitochondrial fusion and fission in cell life and death. Nat. Rev. Mol. Cell Biol. 11 (12), 872–884 (Dec).
Wu, M., Desai, D.H., Kakarla, S.K., Katta, A., Paturi, S., Gutta, A.K., Rice, K.M., Walker Jr., E.M., Blough, E.R., 2009. Acetaminophen prevents aging-associated hyperglycemia in aged rats: effect of aging-associated hyperactivation of p38-MAPK and ERK1/2. Diabetes Metab. Res. Rev. 25 (3), 279–286 (Mar).
Wu, M.H., Lin, C.Y., Hou, C.Y., Sheu, M.T., Chang, H., 2020. Micronized sacchachitin promotes satellite cell proliferation through TAK1-JNK-AP-1 signaling pathway predominantly by TLR2 activation. Chin. Med. 15 (1), 100 (Sep 22).
Xie, Y., Su, N., Yang, J., Tan, Q., Huang, S., Jin, M., Ni, Z., Zhang, B., Zhang, D., Luo, F., Chen, H., Sun, X., Feng, J.Q., Qi, H., Chen, L., 2020. FGF/FGFR signaling in health and disease. Signal Transduct Target Ther. 5 (1), 181 (Sep 2).
Xu, B., Liu, C., Zhang, H., Zhang, R., Tang, M., Huang, Y., Jin, L., Xu, L., Hu, C., Jia, W., 2021. Skeletal muscle-targeted delivery of Fgf6 protects mice from diet-induced obesity and insulin resistance. JCI Insight. 6 (19), e149969 (Oct 8).
Yamakawa, H., Kusumoto, D., Hashimoto, H., Yuasa, S., 2020. Stem cell aging in skeletal muscle regeneration and disease. Int. J. Mol. Sci. 21 (5), 1830 (Mar 6).
Yunna, C., Mengru, H., Lei, W., Weidong, C., 2020. Macrophage M1/M2 polarization. Eur. J. Pharmacol. 15 (877), 173090 (Jun).
Zaarur, N., Meriin, A.B., Bejarano, E., Xu, X., Gabai, V.L., Cuervo, A.M., Sherman, M.Y., 2014. Proteasome failure promotes positioning of lysosomes around the aggresome via local block of microtubule-dependent transport. Mol. Cell. Biol. 34 (7), 1336–1348 (Apr).
Zeltz, C., Gullberg, D., 2016. The integrin-collagen connection–a glue for tissue repair? J. Cell Sci. 129 (4), 653–664 (Feb 15).
Zhang, Y., Zhang, J., Wang, S., 2021. The role of rapamycin in healthspan extension via the delay of organ aging. Ageing Res. Rev. 70, 101376 (Sep).
Zhou, Q., Wan, Q., Jiang, Y., Liu, J., Qiang, L., Sun, L., 2020. A landscape of murine long non-coding RNAs reveals the leading transcriptome alterations in adipose tissue during aging. Cell Rep. 31 (8), 107694 (May 26).